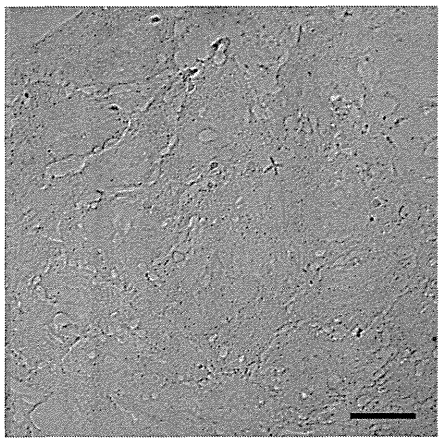

Fig. 5. Phase-contrast image of the Caco-2-cells. The scale bar represents 20 μm.

also be used as excipients of solid oral dosage forms and other products that are absorbed in a body in a variety of ways.

In solid oral dosage form, silicates are commonly used as glidants. Although the primary particle size of the most frequently used colloidal silica (Aerosil 200) is between 7 and 40 nm, these particles group together into so-called aggregates of a few hundred nanometers during the sintering production process [26]. This study therefore investigated the size and in vitro behavior using gastrointestinal models; the Caco-2 cell models and bio-relevant dissolution media simulated conditions in the gastrointestinal system, allowing an evaluation of the intestinal permeability properties and the intestinal cell toxicity associated with oral administration. The critical question regarding the safety of oral dosage forms is whether the material used as an excipient will penetrate the intestinal barrier of the intestinal membrane.

We used fluorescently labeled silica particles to trace the intake and the translocation of the intestinal barrier. The silica particles consisted of amorphous and nonporous silicates, and had a negative charge (Table 1); these characteristics are the same as those of silicates frequently used in solid oral dosage form (approximately −40 mV in

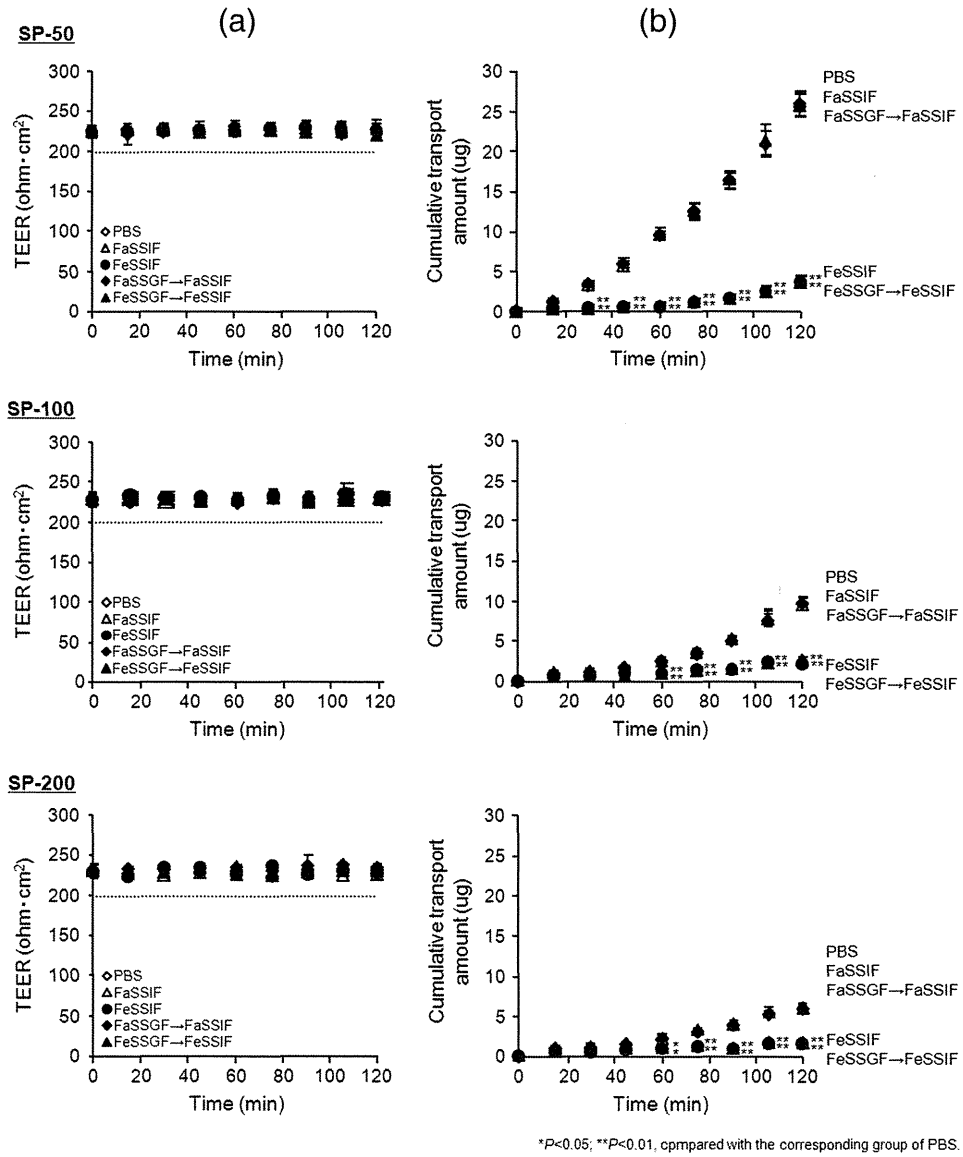

Fig. 6. Trans-epithelial electrical resistance across Caco-2 cell monolayers (a), and cumulative transported amounts of amorphous silica particles (b). SP-50, SP-100, and SP-200 were dispersed in various types of fluids to a final concentration of 1 mg/mL and pre-incubated at 37 °C for 1 h. The incubated fluorescently labeled silica particles were added to the apical side of the Caco-2 cell monolayer. After indicated duration, TEER and the transported amount of nanoparticles were measured as described in "Materials and methods". $^{*}P < 0.05$, $^{**}P < 0.01$, compared with the corresponding group of " PBS". Each value represents the mean ± S.D. ($n = 4$).

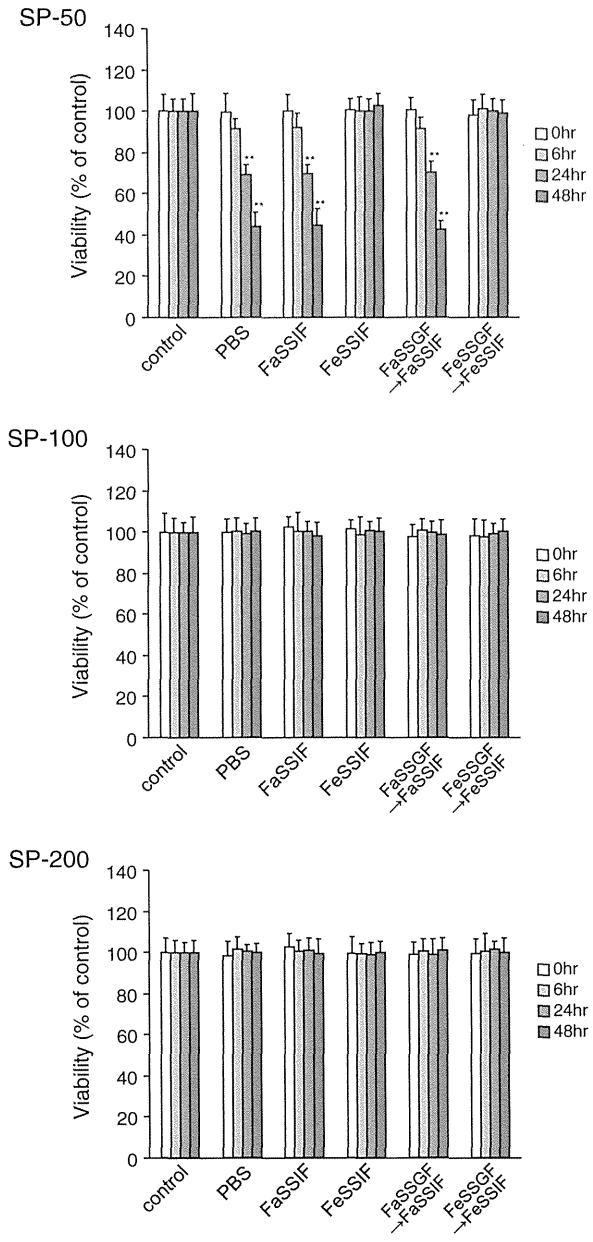

Fig. 7. The cytotoxicity of amorphous silica particles against Caco-2 cells. Silica nanoparticles (final concentration 1.0 mg/mL) were dispersed in various types of fluids and pre-incubated at 37 °C for 1 h. In addition, to mimic the gastric and intestinal conditions (indicated as "FaSSGF → FaSSIF" and "FeSSGF → FeSSIF"), silica particles were diluted to 10 mg/mL in FaSSGF or FeSSGF, incubated at 37 °C for 1 h, and the diluted silica particles were subsequently further diluted to concentrations of 1.0 mg/mL in FaSSIF or FeSSIF, and incubated at 37 °C for an additional 1 h. The pre-incubated particles were added to the cells. After incubation for 6 h, the cultured media was then replaced with fresh medium to eliminate the effect of the fluid itself, and the cells were incubated for another 0, 6, 24, and 48 h. Cell viability was evaluated by using the WST-8 assay at each time point (0, 6, 24, and 48 h). $^{**}P < 0.01$, compared with the corresponding control group. Each value represents the mean ± S.D. ($n = 4$).

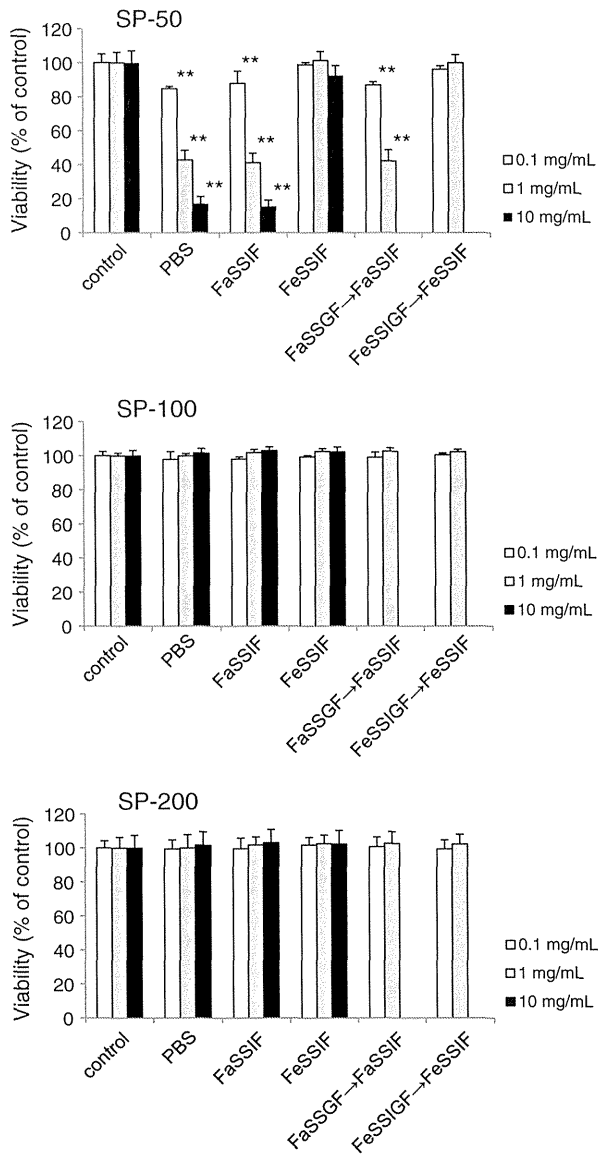

Fig. 8. The concentration dependency of the silica particle toxicity on Caco-2 cells. SP-50, SP-100, and SP-200 (final concentration 0.1, 1.0, and 10 mg/mL) were dispersed in various types of fluids and pre-incubated at 37 °C for 1 h. In addition, to mimic the gastric and intestinal conditions (indicated as "FaSSGF → FaSSIF" and "FeSSGF → FeSSIF"), silica particles were diluted to 10 mg/mL in FaSSGF or FeSSGF, incubated at 37 °C for 1 h, and the diluted silica particles were subsequently further diluted to concentrations of 0.1 or 1.0 mg/mL in FaSSIF or FeSSIF, and incubated at 37 °C for an additional 1 h. The pre-incubated particles were added to the cells. After incubation for 6 h, the cultured media was then replaced with fresh medium to eliminate the effect of the fluid itself, and an additional 48 h of incubation was applied, followed by measurement of cytotoxicity. $^{**}P < 0.01$, compared with the corresponding control group. Each value represents the mean ± S.D. ($n = 4$).

water at pH 7 [27]). We also investigated the size dependence of the absorption and the in vitro toxicity, using silica particles with diameters of 50, 100, and 200 nm.

First, we investigated whether the silica particles would agglomerate after oral administration. Simulation of gastrointestinal conditions is essential to adequately predict the in vivo behavior of drug formulations. We used biorelevant dissolution media that can be used for the in vitro simulation of different dosing conditions (fasted and fed states) [28]. Regardless of the primary particle size, the observed tendency was the same. In all cases, the particles formed agglomerates in the medium representing the fed-state intestinal fluid. It is known that acidic conditions promote agglomeration, due to a decrease in the electrostatic repulsion between negatively charged silica particles; the formation of agglomerates can therefore occur after passage through the stomach, which has lower-pH conditions. However, in this case, lower-pH conditions did not cause agglomeration, under fed or fasted conditions. Furthermore, the viscosity of the FaSSGF = 0.688 mPa s and FeSSGF = 0.704 mPa s were almost the same, which suggested that the viscosity did not affect the agglomeration of the silica particles. Judging from the composition of the bio-relevant dissolution media, and the above results, we concluded that the high salt concentration was a major factor causing the agglomeration. In fact, we reported previously

that silica particles easily agglomerated with high sodium ion concentrations in solution eluents [29], and the same phenomenon was also reported by other researchers [30]. The Derjaguin Landau_Verwey_Overbeek (DLVO) theory is often used to explain the aggregation/agglomeration behavior of silica suspensions [31,32]. Briefly, the DLVO theory combines the effects of the attractive van der Waals forces and the electrostatic repulsion between charged surfaces. As discussed earlier, the presence of silanol groups (Si–O–H) on amorphous silica surfaces and the charge of silanol groups determine the extent of the repulsive energy needed to keep the silica nanoparticles dispersed. The surface charge of silica nanoparticles differs as the pH changes due to protonation and deprotonation of the silanol groups. At pH 2–3, silica nanoparticles reach the isoelectric point (IEP) where the particles carry no net charge, causing the nanoparticles to agglomerate. In the case of biological conditions with high (0.1–0.3 M) salt concentrations, ion-specific effects also play a prominent role [33]. Amiri et al. pointed out that in aqueous media, because pure particles are electrostatically stabilized, interparticle interactions at a given concentrations can be changed by varying the ionic strength, particle size, and pH of the suspension; they demonstrated that high salt concentration causes agglomeration of silica particles [27].

Next, we studied the cellular uptake of silica particles, using Caco-2 cells as an in vitro model to assess the barrier integrity/permeability effects of the silica particles. The TEER, which is well known as an indicator of the integrity of junctions, was not affected by the addition of SP-50, SP-100, or SP-200 under these experimental conditions, suggesting that the silica particles used in this study did not significantly change the structure of the tight junctions between the cells in the Caco-2 cell monolayer, regardless of the particle size, at least for 2 h of exposure to the particles. Because the length of the tight junction between the cells is approximately 10–20 nm [25], the silica particles used in this study did not penetrate the junction. Therefore, the increase in the amount of particles showed that translocation through the Caco-2 cells occurred. The transport experiments showed that the cumulative number of transported silica particles increased with exposure time, and it is notable that translocation occurred under conditions that did not cause agglomeration. In the investigation of the cumulative amount of transported silica particles, Fig. 6 showed that the transported amounts of SP-50 were much higher than those of SP-100 and 200 when these silica particles were dispersed in PBS and FaSSIF. Moreover, the transported amounts of all of the silica particles were significantly lower when they were dispersed in FeSSIF than when they were dispersed in PBS or FaSSIF. However, in the case of SP-100 and SP-200, the amounts of silica particles transported were negligible for times shorter than 1 h, regardless of which fluid was used. Because the transit time in the gut is approximately 1 h per 1 m of gut length [34], these results suggest that the intestinal absorption of silica particles or aggregates/agglomerates larger than 100 nm would be negligible. Further in vivo testing would be necessary to confirm the possibility of silica particle absorption into the systemic circulation.

We then investigated the cytotoxicity of the silica particles towards Caco-2 cells. We confirmed that the exposure for 6 h to the silica particles (SP-50,100, and 200) did not induce cytotoxicity in any of the various types of fluids, and this coincides with our results that the structure of the tight junctions of Caco-2 monolayer was not changed at least for 2 h of exposure to the silica particles (Fig. 6). However, after another incubation with fresh medium, SP-50 showed time-dependent toxicity for up to 48 h when SP-50 was dispersed in PBS or fasted-state simulated fluids. On the other hand, SP-100 and SP-200 did not show any cytotoxicity, at least for 48 h (Fig. 7). The time lapse of toxicity observed in SP-50 in this study indicates that the smaller size of silica particles inhibited cellular proliferation, which has also been reported by Nabeshi et al. [35]. They showed the size-dependent cytotoxic effects of amorphous silica particles (70, 300, and 1000 nm) on mouse epidermal Langerhans cells. The smallest particles induced greater cytotoxicity and inhibited cellular proliferation [35]. We investigated the concentration dependency of silica particles on Caco-2 cells and found that SP-50 was cytotoxic. No cytotoxicity was observed, however, for SP-100 or SP-200, in any of the various types of fluids, even at a concentration of 10 mg/mL (Fig. 8). By contrast, when SP-50 was dispersed in PBS or fasted-state simulated fluids, significant cytotoxicity was detected for all concentrations of the particles, with increasing cytotoxicity as the silica concentration increased. Although SP-100 and 200 were also internalized in the Caco-2 cells in the fasted state, cytotoxicity was not observed.

The size-dependent toxicity of amorphous nanosilica has been also reported by other researchers [16]. The relationship between cytotoxicity and particle sizes observed in our study has been discussed previously by others. Yu et al. examined the cytotoxic activity of well-dispersed amorphous silica particles (30–535 nm) in mouse keratinocytes [36]. All sizes of particles were taken up into the cell cytoplasm. The toxicity was dose- and size-dependent, with 30- and 48-nm particles being more cytotoxic than 118- and 535-nm particles. Nabeshi et al. showed the size-dependent cytotoxic effects of amorphous silica particles (70, 300, and 1000 nm) on mouse epidermal Langerhans cells [35]. They found that the smallest particles induced the greatest cytotoxicity and inhibited cellular proliferation. These observed effects were associated with the quantity of particle uptake into the cells. This association was also present in our study, where the cytotoxicity of SP-50 correlated with the concentration (Fig. 8). Yang et al. evaluated the effects of amorphous silica particles (15 and 30 nm) on cellular viability, the cell cycle, and apoptosis in the human epidermal keratinocyte cell line HaCaT [37]. Their microscopic examination revealed morphological changes after 24-h exposures. Cell growth also appeared to be significant inhibited, and the smaller silica particles were more cytotoxic and induced a higher rate of apoptosis. Oberdörster et al. argued that since smaller particles have a bigger surface area per unit of mass, the surface area is a pivotal factor for the displayed biological activity [38]. The mechanisms by which silica particles exert their cytotoxic effects are still largely unknown, and recent research illustrates the complexity in identifying the hazards of nanoparticles for human health [39]. However, there are many possibilities, including damage to the plasma membrane before particles penetrate the cells, intracellular interference after uptake in late or lysosomal structures, and lysosomal escape [16]. Another research indicated that the effect of silica nanoparticles on HT-29 cells is mediated by the interference with the signaling pathway such as MAPK/ERK1/2 [40].

Our study showed that when SP-50 was dispersed in FeSSIF, large agglomerates were formed, and cytotoxicity was not observed. This indicated that even if the primary particle size was less than 100 nm, the cytotoxicity was largely affected by the agglomerate formation.

Guidance for the assessment of risks associated with the application of nanoscience and nanotechnologies in the food and feed chain [41] recommends in vitro tests, including assessments of the effect of particles on the integrity of the gastrointestinal barriers. Our studies proposed one model to assess the integrity/permeability of the gastrointestinal barrier, and the cytotoxicity based on differentiated Caco-2 cells. Parameters such as the cell viability and the TEER can be also considered to be recommended in the guidance.

5. Conclusions

In the present study, we developed the in vitro assay systems including cellular uptake, transport study, and cytotoxicity study models using Caco-2 cells and simulated gastrointestinal fluids to help the evaluation of the intestinal permeability properties and intestinal cell toxicity of silica particles after they were administered orally. Our study showed that the agglomeration of silica particles was affected by the diet and gastrointestinal fluids. Our study also indicated that there was no significant penetration of silica particles through in vitro models (Caco-2 cells), and the cytotoxicity was not observed if the mean size was larger than 100 nm. This study further showed that the secondary size, including

the factor of agglomeration, is important to assess the potential harmful effects of silica particles on Caco-2 cells. Even when the primary particle size was less than 100 nm, the cytotoxicity was affected by agglomerate formation. The findings obtained from our study may offer valuable information to evaluate the behavior in the gastrointestinal tracts or safety of medicines or foods containing silica particles as additives.

Supplementary data to this article can be found online at http://dx.doi.org/10.1016/j.bbagen.2013.12.014.

Acknowledgement

This work was supported in part by the Health and Labour Sciences Research Grants from the Ministry of Health, Labour and Welfare of Japan.

References

[1] A.B. Lansdown, A. Taylor, Zinc and titanium oxides: promising UV-absorbers but what influence do they have on the intact skin? Int. J. Cosmet. Sci. 19 (1997) 167–172.
[2] H. Nabeshi, T. Yoshikawa, K. Matsuyama, Y. Nakazato, K. Matsuo, A. Arimori, M. Isobe, S. Tochigi, S. Kondoh, T. Hirai, T. Akase, T. Yamashita, K. Yamashita, T. Yoshida, K. Nagano, Y. Abe, Y. Yoshioka, H. Kamada, T. Imazawa, N. Itoh, S. Nakagawa, T. Mayumi, S. Tsunoda, Y. Tsutsumi, Systemic distribution, nuclear entry, and cytotoxicity of amorphous nanosilica following topical application, Biomaterials 32 (2011) 2713–2724.
[3] A. Kunzmann, B. Andersson, T. Thurnherr, H. Krug, A. Scheynius, B. Fadeel, Toxicology of engineered nanomaterials: focus on biocompatibility, biodistribution, and biodegradation, Biochim. Biophys. Acta 1810 (2011) 361–373.
[4] A.M. Nyström, B. Fadeel, Safety assessment of nanomaterials: implications for nanomedicine, J. Control. Release 161 (2012) 403–408.
[5] M. Ferrari, Cancer nanotechnology: opportunities and challenges, Nat. Rev. Cancer 5 (2005) 161–171.
[6] Y. Malam, M. Loizidou, A.M. Seifalian, Liposomes and nanoparticles: nanosized vehicles for drug delivery in cancer, Trends Pharmacol. Sci. 30 (2009) 592–599.
[7] N. Nishiyama, K. Kataoka, Current state, achievements, and future prospects of polymeric micelles as nanocarriers for drug and gene delivery, Pharmacol. Ther. 112 (2006) 630–648.
[8] R.A. Petros, J.M. DeSimone, Strategies in the design of nanoparticles for therapeutic applications, Nat. Rev. Drug Discov. 9 (2010) 615–627.
[9] C.M. Hentzschel, M. Alnaief, I. Smirnova, A. Sakmann, C.S. Leopold, Tableting properties of silica aerogel and other silicates, Drug Dev. Ind. Pharm. 38 (2012) 462–467.
[10] L. Jia, J. Shen, Z. Li, D. Zhang, Q. Zhang, G. Liu, D. Zheng, X. Tian, In vitro and in vivo evaluation of paclitaxel-loaded mesoporous silica nanoparticles with three pore sizes, Int. J. Pharm. 445 (2013) 12–19.
[11] H. Miura, M. Kanebako, H. Shirai, H. Nakao, T. Inagi, K. Terada, Influence of particle design on oral absorption of poorly water-soluble drug in a silica particle–supercritical fluid system, Chem. Pharm. Bull. 59 (2011) 686–691.
[12] M.D. Popova, A. Szegedi, I.N. Kolev, J. Mihaly, B.S. Tzankov, G.T. Momekov, N.G. Lambov, K.P. Yoncheva, Carboxylic modified spherical mesoporous silicas as drug delivery carriers, Int. J. Pharm. 436 (2012) 778–785.
[13] P.J. Borm, D. Robbins, S. Haubold, T. Kuhlbusch, H. Fissan, K. Donaldson, R. Schins, V. Stone, W. Kreyling, J. Lademann, J. Krutmann, D. Warheit, E. Oberdorster, The potential risks of nanomaterials: a review carried out for ECETOC, Part. Fibre Toxicol. 3 (2006) 11.
[14] K.M. Waters, L.M. Masiello, R.C. Zangar, B.J. Tarasevich, N.J. Karin, R.D. Quesenberry, S. Bandyopadhyay, J.G. Teeguarden, J.G. Pounds, B.D. Thrall, Macrophage responses to silica nanoparticles are highly conserved across particle sizes, Toxicol. Sci. 107 (2009) 553–569.
[15] T. Hirai, T. Yoshikawa, H. Nabeshi, T. Yoshida, S. Tochigi, K. Ichihashi, M. Uji, T. Akase, K. Nagano, Y. Abe, H.K. amada, N. Itoh, S. Tsunoda, Y. Yoshioka, Y. Tsutsumi, Amorphous silica nanoparticles size-dependently aggravate atopic dermatitis-like skin lesions following an intradermal injection, Part. Fibre Toxicol. 9 (2012) 3.
[16] J. Kasper, M.I. Hermanns, C. Bantz, O. Koshkina, T. Lang, M. Maskos, C. Pohl, R.E. Unger, C.J. Kirkpatrick, Interactions of silica nanoparticles with lung epithelial cells and the association to flotillins, Arch. Toxicol. 87 (2012) 1053–1065.
[17] M. Pinto, S. Robine-Leon, M.D. Appay, M. Kedinger, N. Triadou, I. Dussaulx, B. Lacroix, P. Simon-Assmann, K. Haffen, J. Fogh, A. Zweibaum, Enterocyte-like differentiation and polarization of the human colon carcinoma cell line Caco-2 in culture, Biol. Cell 47 (1983) 323–330.
[18] I.J. Hidalgo, T.J. Raub, R.T. Borchardt, Characterization of the human colon carcinoma cell line (Caco-2) as a model system for intestinal epithelial permeability, Gastroenterology 96 (1989) 736–749.
[19] P. Artursson, J. Karlsson, Correlation between oral drug absorption in humans and apparent drug permeability coefficients in human intestinal epithelial (Caco-2) cells, Biochem. Biophys. Res. Commun. 175 (1991) 880–885.
[20] K. Gerloff, C. Albrecht, A.W. Boots, I. Forster, R.P.F. Schins, Cytotoxicity and oxidative DNA damage by nanoparticles in human intestinal Caco-2 cells, Nanotoxicology 3 (2009) 355–364.
[21] N. Reix, A. Parat, E. Seyfritz, R. Van der Werf, V. Epure, N. Ebel, L. Danicher, E. Marchioni, N. Jeandidier, M. Pinget, Y. Frere, S. Sigrist, In vitro uptake evaluation in Caco-2 cells and in vivo results in diabetic rats of insulin-loaded PLGA nanoparticles, Int. J. Pharm. 437 (2012) 213–220.
[22] V. Uskoković, K. Lee, P.P. Lee, K.E. Fischer, T.A. Desai, Shape effect in the design of nanowire-coated microparticles as transepithelial drug delivery devices, ACS Nano 6 (2012) 7832–7841.
[23] E. Jantratid, N. Janssen, C. Reppas, J.B. Dressman, Dissolution media simulating conditions in the proximal human gastrointestinal tract: an update, Pharm. Res. 25 (2008) 1663–1676.
[24] V.G. DeMarco, N. Li, J. Thomas, C.M. West, J. Neu, Glutamine and barrier function in cultured Caco-2 epithelial cell monolayers, J. Nutr. 133 (2003) 2176–2179.
[25] J.M. Anderson, Molecular structure of tight junctions and their role in epithelial transport, News Physiol. Sci. 16 (2001) 126–130.
[26] Evonik Industries: Technical Information No. 1271.
[27] A. Amiri, G. Oye, J. Sjoblom, Influence of pH, high salinity, and particle concentration on stability and rheological properties of aqueous suspensions of fumed silica, Colloids Surf. A Physicochem. Eng. Asp. 349 (2009) 43–54.
[28] S. Klein, The use of biorelevant dissolution media to forecast the in vivo performance of a drug, AAPS J. 12 (2010) 397–406.
[29] K. Sakai-Kato, S. Ota, T. Takeuchi, T. Kawanishi, Size separation of colloidally dispersed nanoparticles using a monolithic capillary column, J. Chromatogr. A 1218 (2011) 5520–5526.
[30] J. Depasse, A. Watillon, The stability of amorphous colloidal silica, J. Colloid Interface Sci. 33 (1970) 430–438.
[31] E.J.W. Verwey, J.T.G. Overbeek, Theory of the Stability of Lyophobic Colloids, Elsevier, Amsterdam, 1948.
[32] B. Derjaguin, L. Landau, Theory of the stability of strongly charged lyophobic sols and of the adhesion of strongly charged particles in solution of electrolytes, Acta Phys.-Chim. 14 (1941) 633–662(URSS).
[33] R. Peters, E. Kramer, A.G. Oomen, Z.E. Rivera, G. Oegema, P.C. Tromp, R. Fokkink, A. Rietveld, H.J. Marvin, S. Weigel, A.A. Peijnenburg, H. Bouwmeester, Presence of nano-sized silica during in vitro digestion of foods containing silica as a food additive, ACS Nano 6 (2012) 2441–2451.
[34] N. Parrott, V. Lukacova, G. Fraczkiewicz, M.B. Bolger, Predicting pharmacokinetics of drugs using physiologically based modeling-application to food effects, AAPS J. 11 (2009) 45–53.
[35] H. Nabeshi, T. Yoshikawa, K. Matsuyama, Y. Nakazato, A. Arimori, M. Isobe, S. Tochigi, S. Kondoh, T. Hirai, T. Akase, T. Yamashita, K. Yamashita, T. Yoshida, K. Nagano, Y. Abe, Y. Yoshioka, H. Kamada, T. Imazawa, N. Itoh, S. Tsunoda, Y. Tsutsumi, Size-dependent cytotoxic effects of amorphous silica nanoparticles on Langerhans cells, Pharmazie 65 (2010) 199–201.
[36] K.O. Yu, C.M. Grabinski, A.M. Schrand, R.C. Murdock, W. Wang, B. Gu, J.J. Schlager, S.M. Hussain, Toxicity of amorphous silica nanoparticles in mouse keratinocytes, J. Nanopart. Res. 11 (2009) 15–24.
[37] X. Yang, J. Liu, H. He, L. Zhou, C. Gong, X. Wang, L. Yang, J. Yuan, H. Huang, L. He, B. Zhang, Z. Zhuang, SiO2 nanoparticles induce cytotoxicity and protein expression alteration in HaCaT cells, Part. Fibre Toxicol. 7 (2010) 1–12.
[38] G. Oberdörster, E. Oberdörster, J. Oberdörster, Nanotoxicology: an emerging discipline evolving from studies of ultrafine particles, Environ. Health Perspect. 113 (2005) 823–839.
[39] J.A. Sergent, V. Paget, S. Chevillard, Toxicity and genotoxicity of nano-SiO2 on human epithelial intestinal HT-29 cell line, Ann. Occup. Hyg. 56 (2012) 622–630.
[40] H. Gehrke, A. Frühmesser, J. Pelka, M. Esselen, L.L. Hecht, H. Blank, H.P. Schuchmann, D. Gerthsen, C. Marquardt, S. Diabaté, C. Weiss, D. Marko, In vitro toxicity of amorphous silica nanoparticles in human colon carcinoma cells, Nanotoxicology 7 (2013) 274–293.
[41] EFSA Scientific Committee, Scientific opinion: guidance on the risk assessment of the application of nanoscience and nanotechnologies in the food and feed chain, EFSA J. 9 (2011) 2140.

molecular pharmaceutics

Article

pubs.acs.org/molecularpharmaceutics

Effects of Liposomal Phospholipids and Lipid Transport-Related Protein on the Intracellular Fate of Encapsulated Doxorubicin

Keita Un,[†] Kumiko Sakai-Kato,*[,†] Toru Kawanishi,[‡] Haruhiro Okuda,[‡] and Yukihiro Goda[†]

[†]Division of Drugs, National Institute of Health Sciences, 1-18-1 Kamiyoga, Setagaya-ku, Tokyo 158-8501, Japan

[‡]National Institute of Health Sciences, 1-18-1 Kamiyoga, Setagaya-ku, Tokyo 158-8501, Japan

Supporting Information

ABSTRACT: We have previously reported the intracellular trafficking mechanism of liposomal phospholipids. In the present study, we investigated the effects of liposomal phospholipids on the intracellular trafficking of doxorubicin (DXR). In DXR-encapsulated liposomes, polyethylene glycol (PEG)-modified phospholipids have been widely used as one of the liposomal lipids. First, we investigated the intracellular trafficking mechanism of 1,2-distearoyl-*sn*-glycero-3-phosphocholine (DSPC) and (1,2-distearoyl-*sn*-glycero-3-phosphoethanolamine-*N*-[methoxy-PEG$_{2000}$] (PEG$_{2000}$-DSPE), and demonstrated that the intracellular trafficking pathways of phospholipids changed by PEG modification. Then, we evaluated the effects of liposomal DXR on the intracellular trafficking of liposomal phospholipids. Under the phosphatidylinositol transfer protein (PITP)-suppressing condition by siRNA treatment, the intracellular amounts of DSPC derived from DXR-encapsulated liposomes were larger than that from nonencapsulated liposomes. Moreover, following the effects of liposomal phospholipids on the intracellular amounts of DXR, the intracellular amounts of DXR were increased under the PITP-suppressing condition in DXR-encapsulated liposomes. We showed that intracellular DXR was associated with the complex of PITP and DSPC, and the extracellular efflux of DXR was enhanced by complex formation with PITP and DSPC.

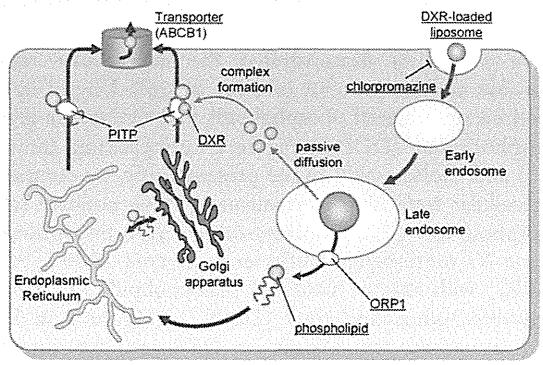

KEYWORDS: *polyethylene glycol-modified liposome, doxorubicin, intracellular trafficking, phosphatidylinositol transfer protein, cytotoxicity*

■ INTRODUCTION

Liposomes composed of a lipid bilayer membrane are frequently used as membrane models or as drug delivery systems. Because the major components of liposomes are phospholipids and cholesterols, liposomes exhibit low cytotoxicity *in vitro* and *in vivo*.[1] However, their instability *in vivo* and their unexpected uptake into components of the reticuloendothelial system (RES), including the liver and spleen, must be considered when using liposomes.[2] Because of these issues, polyethylene glycol (PEG)-modified liposomes containing PEG-modified phospholipids as functional lipids have been developed.[3,4] The adsorption of complements and serum proteins on PEG-modified liposomes was suppressed by the PEG chain on the surface of liposomes.[5] This modification decreases liposomal uptake into RES and increases the retention time in the blood.[6] Because vascular permeability is greater in tumor tissues than in normal tissues, the accumulation of PEG-modified liposomes in tumor tissue and retention time in the blood were much greater than conventional liposomes.[7] Doxorubicin (DXR)-encapsulated PEG-modified liposomes have already been approved in several countries, and this formulation is expected to be a promising drug with enhanced antitumor activity and reduced side effects compared with conventional DXR.[8,9]

Despite these advantages, the aqueous layer formed by PEG modification suppresses interactions between the liposomes and the cell membrane.[10] Therefore, the intracellular uptake of PEG-modified liposomes into the target cells is less than that of conventional liposomes. Some researchers have successfully developed PEG-modified liposomes in which the PEG chain located on the liposomal surface is selectively cleaved in tumor tissues, enhancing effective intracellular drug delivery.[11,12] On the other hand, to date, there have been very few reports describing the intracellular trafficking mechanism of liposomes containing PEG-modified phospholipids. Our research group has evaluated the intracellular trafficking mechanism of block copolymers including a PEG chain, and showed that this amphipathic polymer was effluxed *via* the ATP-binding cassette transporter (ABC) B1, which is also known as P-glycoprotein (P-gp).[13] Because P-gp is involved in the extracellular efflux of various compounds, including anticancer agents, we thought it was important to determine its role in the intracellular

Received: August 23, 2013
Revised: November 18, 2013
Accepted: January 2, 2014
Published: January 2, 2014

trafficking of PEG-modified phospholipids, a group of amphipathic molecules.

Intracellular trafficking of DXR is generally controlled by passive diffusion. Therefore, there are few reports describing the intracellular trafficking of DXR encapsulated in PEG-modified liposomes. DXR induces the expression of various types of intracellular proteins, including the ABC family of transporters.[14−17] ABC transporters are involved in the extracellular efflux of various drugs and liposomal components, including phospholipids and cholesterols. Therefore, it is important to be able to evaluate and predict the intracellular concentrations of DXR, especially to avoid reducing its pharmacological effects and to minimize unexpected toxicity when using encapsulated formulations of DXR. In this context, improved understanding of the intracellular trafficking of DXR is essential to be able to predict the intracellular concentrations of DXR.

We previously demonstrated the intracellular trafficking pathways and the proteins involved in trafficking of liposomes based on unsaturated phospholipids (1,2-dioleoyl-*sn*-glycero-3-phosphocholine [DOPC], Figure 1 in Supporting Information [SI]) and cholesterol.[18] In the present study, we compared the intracellular trafficking mechanism of PEG-modified saturated phospholipids (1,2-distearoyl-*sn*-glycero-3-phosphoethanolamine-*N*-[methoxy(polyethylene glycol)-2000 [PEG_{2000}-DSPE]) with that of saturated phospholipids (1,2-distearoyl-*sn*-glycero-3-phosphocholine [DSPC]) (Figure 1 in SI). We then examined the effects of DXR on the intracellular trafficking of phospholipids *in vitro*. Finally, we evaluated the effects of liposomal phospholipids on the intracellular trafficking and cytotoxicity of DXR.

■ EXPERIMENTAL SECTION

Materials and Cells. DSPC and cholesterol (chol) were purchased from Sigma-Aldrich (St. Louis, MO, U.S.A.). PEG_{2000}-DSPE was obtained from NOF (Tokyo, Japan). DXR was purchased from Wako Pure Chemical Industries (Osaka, Japan). Nitrobenzoxadiazol (NBD)-labeled DSPC and carboxyfluorescein (CF)-labeled PEG_{2000}-DSPE were purchased from Avanti Polar Lipids (Alabaster, AL, U.S.A.), and ATTO 647N-labeled 1,2-dioleoyl-*sn*-glycero-3-phosphoethanolamine (DOPE) was obtained from ATTO-TEC (Siegen, Germany). Dulbecco's-modified Eagle's medium (DMEM), penicillin/streptomycin, phosphate-buffer saline (PBS), and Opti-MEM I were purchased from Life Technologies (Brooklyn, NY, U.S.A.). Fetal bovine serum (FBS) was obtained from Nichirei Biosciences (Tokyo, Japan). All other chemicals used in this study were of the highest purity available. HeLa cells (Health Science Research Resources Bank, Osaka, Japan) were cultured in DMEM supplemented with 10% FBS and 100 U/mL penicillin/streptomycin. Cells were grown in a humidified incubator at 37 °C under 5% CO_2.

Preparation of Liposomes. The liposomes used in this study were prepared according to Bangham's method.[19] Briefly, DSPC, chol, and DSPE-PEG_{2000} were mixed in chloroform, and the mixture was dried by evaporation and vacuum desiccated. The resultant lipid film was resuspended in PBS (pH 7.4) or 250 mM ammonium sulfate (pH 5.4) under mechanical agitation. After hydration for 30 min at 65 °C, the dispersion was sonicated for 10 min in a bath-type sonicator (Sharp Manufacturing Systems, Osaka, Japan) and for 3 min in a tip-type sonicator (Sonics, Newtown, CT, U.S.A.). Then, the liposome solution was sized by repeated extrusion through polycarbonate membrane filters (Avestin, Ottawa, ON, Canada) with a pore size of 100 nm. The particle sizes, polydispersity index (PDI), and ζ-potentials of the liposomes were determined using a Zetasizer Nano ZS (Malvern Instrument, Worcestershire, UK). DXR was loaded into liposomes by the remote-loading method.[20] Briefly, the external phase of liposomes hydrated with 250 mM ammonium sulfate (pH 5.4) was replaced with PBS (pH 8.0) by gel filtration using a Sephadex G-25 column (PD-10; GE Healthcare, Buckinghamshire, UK). DXR dissolved in PBS (pH 8.0) was added to the liposome solution at a drug-to-lipid molar ratio of 1:10 and incubated at 60 °C for 1 h.

Evaluation of Intracellular Trafficking of Liposomes. To evaluate the intracellular concentrations of DSPC and PEG_{2000}-DSPE liposomes, we prepared liposomes containing fluorescence-labeled DSPC and PEG_{2000}-DSPE at a molar ratio of 5%. HeLa cells were plated in 12-well plate (2.5×10^4 cells/well) in DMEM containing 10% FBS and 100 U/mL penicillin/streptomycin. After incubation for 48 h (37 °C, 5% CO_2), liposomes were added to the culture medium. After the indicated times, the cells were washed three times in PBS, trypsinized with 0.25% trypsin-ethylenediamine tetraacetic acid (EDTA) (Life Technologies), washed three times with Hanks' balanced salt solution (HBSS) (Life Technologies), and suspended in lysis buffer (1% Triton X-100 in HBSS). The cell suspension was shaken, centrifuged at 15,000 × g at 4 °C for 10 min, and the fluorescence intensity of resultant supernatant was measured in a fluorescence spectrophotometer (F-7000; Hitachi High-Technologies, Tokyo, Japan). The fluorescence intensity was normalized for the protein content of cells. The protein concentration was determined with a Protein Quantification Kit-Wide Range (Dojindo Laboratories, Kumamoto, Japan).

Confocal Microscopy. To observe the colocalization of endosomes and lysosomes, the cells were washed with HBSS and labeled with AlexaFluor-546-conjugated transferrin (Life Technologies) and LysoTracker Red DND-99 (Life Technologies), respectively. To label the endoplasmic reticulum (ER), Golgi apparatus, and mitochondria, the cells were labeled with ER-Tracker Red (Life Technologies), BODIPY TR C_5-ceramide complexed to BSA (Life Technologies), and Mito-Tracker Red FM (Life Technologies), respectively. HeLa cells (5.0×10^4) were plated in 35-mm glass-bottom dishes coated with poly-L-lysine (Matsunami glass, Osaka, Japan) in DMEM containing 10% FBS and 100 U/mL penicillin/streptomycin. After incubation for 48 h (37 °C, 5% CO_2), liposomes were added to the culture medium. At the indicated times after adding liposomes containing fluorescence-labeled DSPC and PEG_{2000}-DSPE, the cells were washed and placed in PBS for confocal microscopy (LSM 780; Carl Zeiss, Oberkochen, Germany). Images were obtained using dedicated software supplied by the manufacturer and exported as tagged image files.

Evaluation of Endocytosis Inhibition. Endocytosis was inhibited by chlorpromazine (50 μM) to inhibit clathrin-mediated endocytosis, genistein (200 μM) and methyl-β-cyclodextrin (MβCD, 2.0 mM) to inhibit caveolae-mediated endocytosis inhibitor, or 5-(*N*-ethyl-*N*-isopropyl) amiloride (50 μM) to inhibit macropinocytosis.[21,22] Each inhibitor was added to the culture medium 30 min before adding the liposomes.

Small Interfering (si)RNA Transfer. Stealth RNAi oligonucleotides (25 mer) were obtained from Life Technologies. The siRNA sequences used in this study are listed in

Table 1 in SI. The Stealth RNAi High GC Negative Control Duplex (Life Technologies) was used as a negative control. The Stealth RNAi oligonucleotides were transfected into cells using Lipofectamine RNAiMAX (Life Technologies). Cells were incubated with each siRNA for 6 h, after which the culture medium was replaced, and the cells were incubated for a further 42 h before adding the liposomes.

Western Blotting. HeLa cells were washed with PBS and lysed in lysis buffer (20 mM Tris-HCl (pH 7.5), 1 mM EDTA, 10% glycerol, and 1% Triton X-100) containing protease inhibitors (2 mM phenylmethylsulfonyl-fluoride and protease inhibitor cocktail; Sigma-Aldrich). The cell lysates were freeze/thawed and centrifuged at 15000*g* at 4 °C for 10 min. Then, we determined the protein concentration of each supernatant using a Protein Quantification Kit-Wide Range (Dojindo Laboratories). For Western blotting, protein samples (20 μg) were heated to 95 °C for 5 min, diluted with loading buffer, and separated by sodium dodecyl sulfate-polyacrylamide gel electrophoresis using 5–20% polyacrylamide gels (SuperSep Ace; Wako Pure Chemical Industries). The separated proteins were transferred to a polyvinylidene fluoride membrane (Immobilon-P; Millipore, Billerica, MA, U.S.A.) by semidry blotting with a Transblot SD (Bio-Rad, Hercules, CA, U.S.A.). To avoid nonspecific binding, the membrane was incubated with Tris-buffered saline containing 5% enhanced chemiluminescence (ECL) Blocking Agent (GE Healthcare). To detect each protein, the primary and secondary antibodies were diluted in Tris-buffered saline containing 5% ECL Blocking Agent. The protein band was detected using ECL reagents (GE Healthcare).

Evaluation of Cytotoxicity. Cytotoxicity was assessed using a WST-8 assay. HeLa cells were plated in a 96-well plate (5.0×10^3 cells/well) in a medium containing 10% FBS and 100 U/mL penicillin/streptomycin. After preincubation for 48 h (37 °C, 5%CO_2), 50 μg/mL of liposomes was added to the culture medium, and the cells were incubated for the specified times. After incubation, cell counting kit-8 solution (Dojindo Laboratories) was added to each well and incubated for 4 h. Absorbance at 450 nm (test wavelength) and 655 nm (reference wavelength) was measured, and the results are expressed as the relative viability (%).

Confirmation of Complex Formation. HeLa cell lysates were prepared according to the Western Blotting section mentioned above. Then, we determined the protein concentration of each supernatant using a Protein Quantification Kit-Wide Range (Dojindo Laboratories). DSPC liposomes were also prepared using DSPC and NBD-labeled DSPC at a molar ratio of 95:5 in 250 mM ammonium sulfate (pH 5.4) according to the Preparation of Liposomes section. The external phase of liposomes was replaced with PBS (pH 8.0) by gel filtration using a Sephadex G-25 column.

Then, 10 μg of HeLa cell lysates were incubated with 1 μg of DOPC liposomes and 0.1 μg of DXR for 24 h at 37 °C to confirm the complex formation with specific protein, phospholipids, and DXR. The resultant mixture was separated and transferred to a polyvinylidene fluoride membrane according to the Western Blotting section. After the blocking and antibody incubation procedure, the protein band was detected using ECL reagents. The band of detected protein, fluorescence-labeled phospholipids, and DXR was visualized using a LAS-4000 mini-imaging system (FUJIFILM Co., Tokyo, Japan).

Statistical Analyses. Results are presented as the mean ± standard deviation (SD) of at least six experiments. Analysis of variance was used to test for statistically significant differences among groups. Comparisons between two groups were done by the Student's *t*-test, and multiple comparisons between the control and test groups were done using Dunnett's test.

■ RESULTS

Physicochemical Properties. The physicochemical properties of liposomes containing NBD-labeled DSPC or CF-labeled PEG_{2000}-DSPE were determined by measuring the particle sizes, PDI, and ζ-potentials. The mean particle sizes, PDI, and ζ-potentials were approximately 96 nm, 0.08, and 0 mV, respectively (Table 2 in SI).

Intracellular Transport of PEG-Modified Phospholipids. To investigate the intracellular transport mechanisms of PEG_{2000}-DSPE constructing liposomes, the intracellular amounts of CF-labeled PEG_{2000}-DSPE were quantified in HeLa cells. Liposomes were labeled with NBD-labeled DSPC or CF-labeled PEG_{2000}-DSPE, and intracellular uptake into cells was studied by confocal microscopy. DSPC and PEG_{2000}-DSPE were colocalized with endosomes/lysosomes within 1 h of adding each liposome to HeLa cells (Figure 2A in SI). Inhibition of clathrin-mediated endocytosis with chlorpromazine significantly decreased the intracellular concentrations of both lipid components at 2 h after adding the liposomes (Figure 2B in SI).

Intracellular Trafficking Mechanism of PEG-Modified Phospholipids. The intracellular localization of PEG_{2000}-DSPE was compared with that of DSPC by confocal microscopy. As shown in Figure 1, DSPC was colocalized with the ER and Golgi apparatus at 24 h after adding the liposomes to HeLa cells, but was not colocalized with mitochondria (Figure 1, upper panels). By contrast, PEG_{2000}-DSPE was colocalized with the ER, but not with the Golgi apparatus or mitochondria (Figure 1, lower panels).

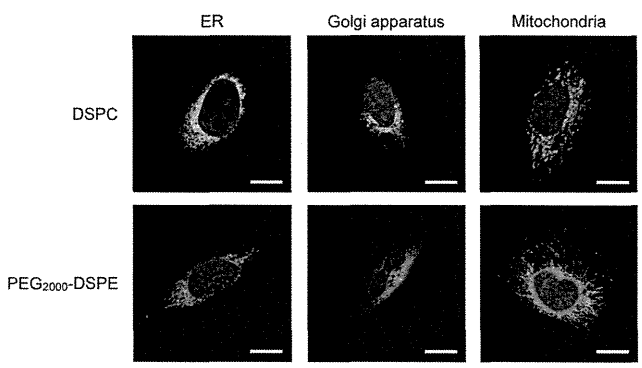

Figure 1. Confocal images showing the intracellular localization of DSPC and PEG_{2000}-DSPE at 24 h after adding liposomes to HeLa cells. Liposomes were labeled with NBD-labeled DSPC (green) or CF-labeled PEG_{2000}-DSPE (green), while the ER, Golgi apparatus, and mitochondria were labeled with ER-Tracker Red (red), BODIPY TR C_5-ceramide (red), and Mito-Tracker Red (red), respectively. Nuclei were counterstained with Hoechst 33342 (blue). Scale bars, 20 μm.

The intracellular trafficking mechanisms of PEG_{2000}-DSPE were compared with that of DSPC. First, we examined the mechanisms controlling trafficking of both phospholipids from the endosome/lysosome to the cytoplasm. In this experiment, suppression of specific proteins using siRNA increased the

intracellular concentrations of phospholipids. In particular, when we suppressed the expression of lipidic trafficking-related proteins, including metastatic lymph-node gene 64 (MLN64) protein, Niemann-Pick C (NPC)1, NPC2, and oxysterol-binding protein-related protein (ORP) 1 (Figure 3 in SI),[23−26] we found that the intracellular concentrations of both phospholipids at 24 h after the addition of liposomes were increased by the suppression of ORP1 (Figure 2A).

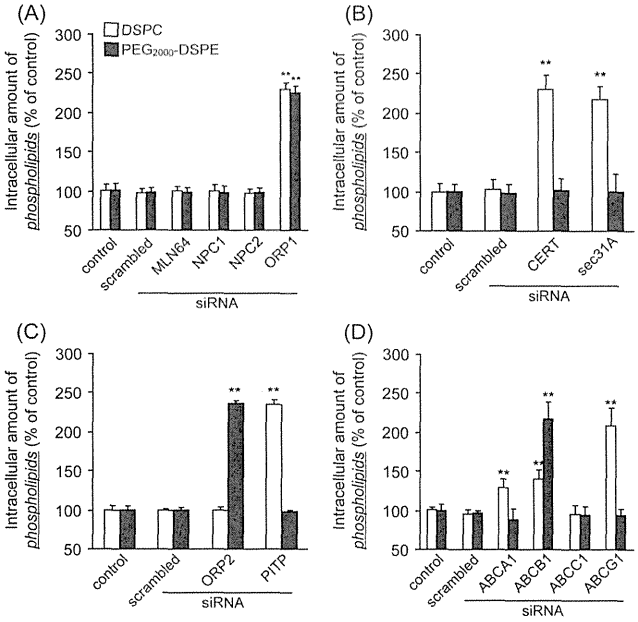

Figure 2. Intracellular trafficking mechanism of DSPC and PEG_{2000}-DSPE in HeLa cells. The intracellular concentrations of DSPC and PEG_{2000}-DSPE were measured 24 h after adding the liposomes to HeLa cells following the suppression of trafficking proteins. siRNAs were used to suppress the expression of proteins involved in the intracellular trafficking from the endosome/lysosome to the cytoplasm (MLN64, NPC1, NPC2, and ORP1) (A), ER−Golgi transport (CERT and sec31A) (B), intracellular trafficking from the ER/Golgi apparatus to the cell membrane (ORP2 and PITP) (C), and extracellular efflux (ABCA1, ABCB1, ABCC1, and ABCG1) (D). siRNAs were transfected using Lipofectamine RNAiMAX. $^{**}P < 0.01$ vs the corresponding control group. Values are presented as mean ± SD ($n = 6$).

Next, we examined the involvement of ER−Golgi transport in the intracellular trafficking of PEG_{2000}-DSPE and DSPC. Suppression of ceramide-transfer protein (CERT) and sec31A, two ER−Golgi transport-related proteins (Figure 3 in SI),[27,28] increased the intracellular concentrations of DSPC at 24 h after adding the liposomes but did not affect the intracellular concentrations of PEG_{2000}-DSPE (Figure 2B).

Then, we investigated the extracellular efflux mechanism of DSPC and PEG_{2000}-DSPE in HeLa cells. To determine the trafficking mechanism from the ER/Golgi apparatus to the cell membrane, we suppressed the expression of ORP2 and phosphatidylinositol transfer protein (PITP), which are involved in the intracellular transport of lipidic molecules (Figure 3 in SI).[29,30] Suppression of ORP2 increased the intracellular concentration of PEG_{2000}-DSPE, but not DSPC, at 24 h after the addition of liposomes (Figure 2C). In experiments in which we suppressed the expression of the ABC transporters (ABCA1, ABCB1, ABCC1, and ABCG1),[31] we found that suppression of ABCB1, but not the other transporters, increased the intracellular concentrations of PEG_{2000}-DSPE at 24 h after the addition of liposomes (Figure 2D). By contrast, only the suppression of ABCG1 increased the intracellular concentrations of DSPC (Figure 2D).

Effects of Liposomal DXR on the Intracellular Trafficking of Phospholipids. We next determined the effects of encapsulating drugs into liposomes on the intracellular trafficking of phospholipids. In this study, we used DXR as the encapsulated drug because it is already clinically used as an anticancer agent in free or liposomal forms.[32] First, we evaluated the effects of DXR on the expression of intracellular trafficking-related proteins in HeLa cells. As shown in Figure 3A, exposure to 0.1 μM DXR for 24 h increased the intracellular expression levels of PITP, ABCA1, and ABCB1 (0.1 μM).

We then investigated the effects of DXR on intracellular trafficking of liposomes generated using phospholipids. In this experiment, we focused on the intracellular proteins whose expression was increased by DXR (i.e., PITP, ABCA1, and ABCB1). As the clinical formulation of liposomal DXR is generated by encapsulating DXR into PEG-modified liposomes,[32] we used PEG-modified liposomes as the model liposomes, and we measured the intracellular concentrations of DSPC, the major component of liposomes. The molar ratio of DSPC, chol, and PEG_{2000}-DSPE was 45:50:5, and the DXR loading efficiency and mean particle size were approximately 96% and 100 nm, respectively. Figure 3B shows that suppression of PITP expression, a protein involved in intracellular transport from the ER/Golgi apparatus to the cell membrane (Figure 3 in SI), resulted in greater intracellular concentrations of phospholipids derived from DXR-loaded liposomes as compared with phospholipids derived from unloaded liposomes. Regarding extracellular efflux, the intracellular concentrations of phospholipids derived from DXR-loaded liposomes were higher than that of phospholipids from unloaded liposomes when we suppressed the expression of ABCA1 and ABCB1 (Figure 3C).

Effects of Lipid Components on Intracellular Trafficking and the Cytotoxicity of DXR. We finally examined the effects of liposomes generated using phospholipids on the intracellular transport of DXR. In these experiments, we used PEG-modified liposomes as the model liposomes. Suppression of proteins involved in endosome/lysosome cytoplasm transport or ER−Golgi transport did not affect the intracellular concentrations of DXR transported by PEG-modified liposomes (data not shown). As shown in A and B of Figure 4, the intracellular concentrations of DXR transported by PEG-modified liposomes was increased when the expression of PITP and ABCB1 was suppressed. Moreover, the cytotoxicity of DXR transported by PEG-modified liposomes was increased by suppressing PITP and ABCB1 expression in HeLa cells (Figure 4C). Similar results were obtained in the experiments using DXR transported by unmodified liposomes (data not shown).

The increase in intracellular concentration of DXR after suppressing ABCB1 expression is attributed to the previous reports that DXR is the substrate of ABCB1.[33−35] By contrast, although PITP is involved in the intracellular transport of phospholipids (Figure 2C), PITP was not involved in the intracellular trafficking of DXR (Figure 4 in SI).

Next, we investigated the formation of complexes of PITP, phospholipids, and DXR. After incubation in various conditions aimed at promoting complex formation, we found that DSPC formed a complex with PITP, but DXR did not form a complex

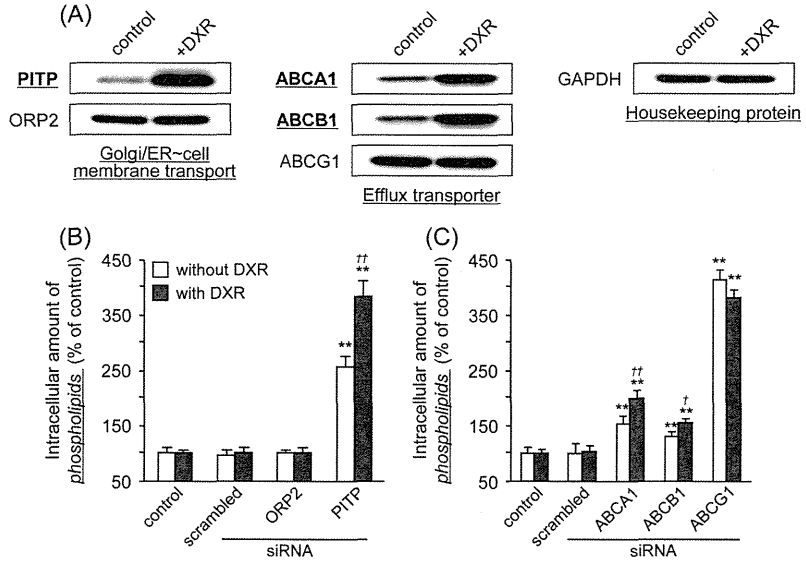

Figure 3. Effects of DXR-encapsulated liposomes on the intracellular trafficking of phospholipids in HeLa. (A) Effects of DXR on the expression of proteins involved in intracellular trafficking of phospholipids. Cells were incubated for 24 h in the presence of a low concentration of DXR (0.05 μg/mL) and protein expression was determined by Western blotting. (B, C) Intracellular concentrations of phospholipids at 24 h after adding liposomes to HeLa cells with suppression of trafficking-related proteins. Liposomes were labeled with ATTO-647N DOPE. siRNAs were used to suppress the expression of proteins involved in intracellular trafficking from the ER/Golgi apparatus to the cell membrane (ORP2 and PITP) (B), or extracellular efflux (ABCA1, ABCB1, and ABCG1) (C). siRNAs were transfected using Lipofectamine RNAiMAX. $^{**}P < 0.01$ vs the corresponding control group; $^{\dagger}P < 0.05$; $^{\dagger\dagger}P < 0.01$ vs the DXR-untreated group. Values are presented as mean ± SD ($n = 6$).

with PITP (Figure 4D). However, DXR did form a complex with PITP in the presence of DSPC (Figure 4D). Moreover, as shown in Figure 4E, the intracellular concentrations of DXR increased when PITP expression was suppressed following coincubation with DSPC liposomes. These observations suggest that DXR transported by liposomes forms complexes with PITP and phospholipids, and this complex is involved in the intracellular trafficking of transported DXR.

■ DISCUSSION

In this study, we first investigated the intracellular trafficking of PEG-modified phospholipids used to generate liposomes. We have previously reported on the intracellular trafficking mechanism of phospholipids and chols, the major components of liposomes.[18] In this study, we evaluated the effects of PEG modification on the intracellular trafficking of phospholipids. As shown in Figure 1, following intracellular uptake of PEG-modified DSPE *via* endocytosis, although DSPC was localized to the ER and Golgi apparatus, PEG-modified DSPE was only localized to the ER. Moreover, the intracellular concentrations of PEG_{2000}-DSPE were not affected by suppressing CERT and sec31A expression (Figures 2B), suggesting that ER–Golgi transport is not involved in the intracellular trafficking of PEG-modified phospholipids. Although DSPC was transported to the cell membrane by PITP and extracellular effluxed *via* ABCG1, PEG-modified DSPE was transported to the cell membrane by ORP2 and extracellular effluxed *via* ABCB1 (Figures 2C and 2D). Thus, we showed that PEG modification had remarkable effects on the intracellular trafficking of phospholipids.

Next, we evaluated the effects of encapsulating drugs into liposomes on the intracellular trafficking of liposomal phospholipids. In this series of experiments, we used DXR as the encapsulated drug because it is widely used as an anticancer agent, and liposomal formulations are in clinical use.[32] We found that exposure to a low concentration of DXR for 24 h increased the expression of PITP, ABCA1, and ABCB1 in HeLa cells (Figure 3A). Furthermore, the intracellular concentrations of liposomal phospholipids derived from DXR-loaded liposomes were increased by the suppression of PITP expression (Figure 3B). These results suggest that DXR enhances the extracellular efflux of liposomal phospholipids by enhancing PITP expression. We also found that the intracellular concentrations of liposomal phospholipids were increased by DXR following suppression of ABCA1 and ABCB1 expression (Figure 3C). These findings suggest that DXR enhances the activities of ABCA1 and ABCB1 in terms of extracellular efflux of phospholipids. It was previously reported that low concentrations of DXR induce the expression of various ABC transporters.[14−17] Therefore, our results suggest that DXR encapsulated into liposomes enhances ABCA1 and ABCB1 expression, which consequently increases the extracellular efflux of phospholipids. Various anticancer agents were reported to enhance the expression of ABC transporters, including P-gp.[14−17] In a previous study[18] and the present study, we showed that the major liposomal components underwent extracellular efflux *via* ABC transporters, and competitively inhibited ABC transporter-mediated extracellular efflux of encapsulated drugs.[18] Considering these findings, we think that, although DXR increases the expression of P-gp, the extracellular efflux of DXR *via* P-gp will be suppressed by competitive inhibition of P-gp by phospholipids. These events might ultimately enhance the anticancer effects of DXR .

We also investigated the effects of liposomal phospholipids on the intracellular trafficking and cytotoxicity of DXR. In experiments aimed at determining the effects of various proteins on DXR trafficking, we found that the intracellular concentrations of DXR were only increased when we suppressed ABCB1 expression (Figure 4 in SI). These results are consistent with those of earlier reports showing that DXR is

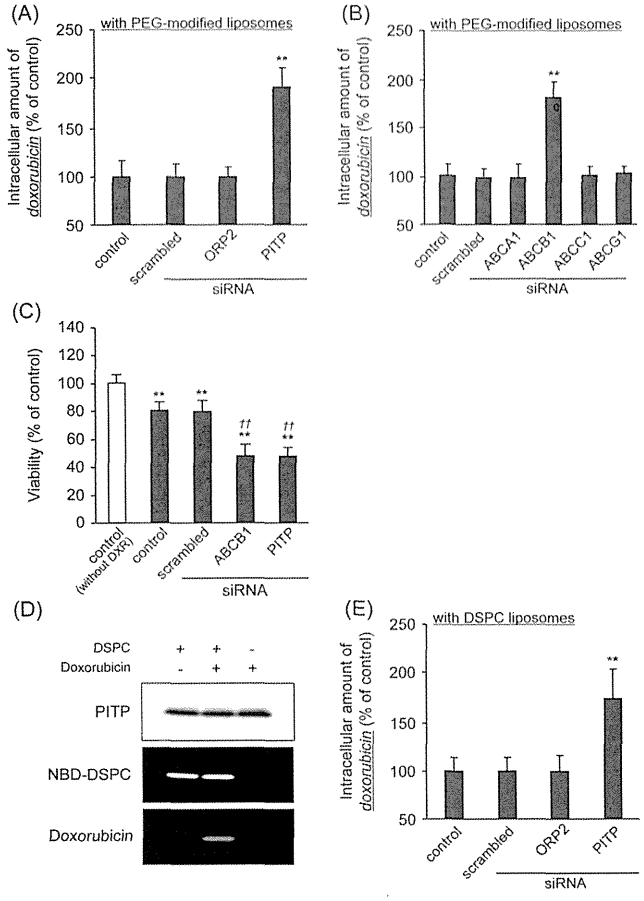

Figure 4. Effects of lipid components on intracellular trafficking and cytotoxicity of DXR. (A, B) Intracellular concentrations of DXR encapsulated in PEG-modified liposomes 24 h after adding the liposomes to HeLa cells with suppression of trafficking-related proteins. siRNAs were used to suppress the expression of proteins involved in the intracellular trafficking of phospholipids from the ER/Golgi apparatus to the cell membrane (ORP2 and PITP) (A) and the extracellular efflux (ABCA1, ABCB1, ABCC1, and ABCG1) (B). $^{**}P < 0.01$ vs the corresponding control group. Values are presented as mean ± SD ($n = 6$). (C) Cytotoxicity of DXR encapsulated in PEG-modified liposomes in HeLa cells with suppression of PITP and ABCB1 expression. Cytotoxicity was evaluated using a WST-8 assay. $^{**}P < 0.01$ vs the corresponding control group lacking DXR; $^{\dagger\dagger}P < 0.01$ vs the corresponding control group. Values are presented as mean ± SD ($n = 6$). (D) Evaluation of complexes of PITP, phospholipids, and DXR. Liposomes generated using NBD-labeled DSPC (1.0 μg) and DXR (0.1 μg) were mixed with HeLa cell lysates containing PITP (10 μg protein). (E) Intracellular concentrations of DXR at 24 h after adding liposomes to HeLa cells with suppression of ORP2 and PITP expression. $^{**}P < 0.01$ vs the corresponding control group. Values are presented as mean ± SD ($n = 6$).

a substrate of ABCB1.[33−35] However, when cells were treated with DXR encapsulated in PEG-modified liposomes, we found that the intracellular concentrations of DXR were increased by the suppression of ABCB1 and PITP expression (Figures 4A and 4B). In fact, suppression of ABCB1 and PITP expression increased the cytotoxicity of DXR encapsulated in PEG-modified liposomes in HeLa cells (Figure 4C). These observations suggest that PITP is involved in the intracellular trafficking of liposome-encapsulated DXR. Although, several reports have shown that PITP is involved in the transport of phosphatidylcholine and phosphatidylinositol,[29,36,37] there are no reports showing that PITP is involved in DXR transport. Therefore, we evaluated the formation of complexes of PITP, liposomal phospholipids, and DXR. As shown in Figures 4D and 4E, DXR formed a complex with PITP in the presence of phospholipids, and the intracellular concentration of DXR increased following suppression of PITP expression and preincubation with phospholipids. These results indicate that the intracellular trafficking of DXR released from liposomes to the endosome/lysosome is controlled by PITP, which forms a complex with phospholipids and DXR released from DXR-encapsulated liposomes (Figure 5).

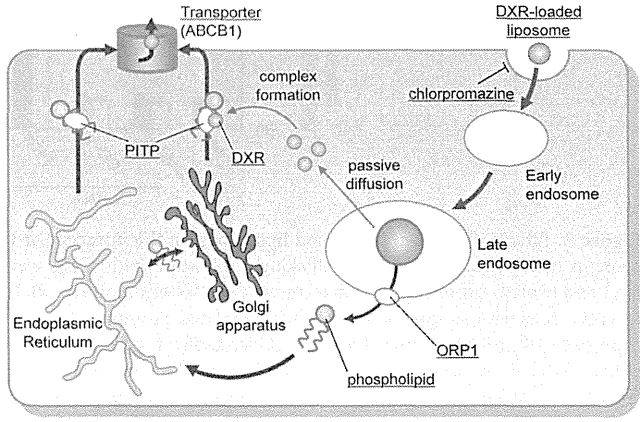

Figure 5. Predicted mechanism of the intracellular trafficking of liposome-encapsulated DXR.

It is known that the intracellular trafficking of DXR is controlled by passive diffusion. Therefore, while several studies have focused on the intracellular uptake process of DXR encapsulated into liposomes,[12,38,39] few have described the intracellular trafficking after intracellular uptake. Here, we showed that DXR forms a complex with PITP and phospholipids, and that DXR was subject to intracellular trafficking as a complex in cells exposed to DXR-encapsulated liposomes. To our knowledge, there are no reports showing that liposomal lipids and encapsulated drugs form a complex with specific intracellular proteins, or that the intracellular trafficking of drugs requires complex formation. These findings demonstrate the importance of elucidating the interactions between encapsulated drugs and other intracellular proteins/liposomal components in order to improve the pharmacological activities and safety of encapsulated drugs.

It well-known that PITP is involved in the intracellular trafficking of phospholipids from the ER/Golgi apparatus to the cell membrane.[29,36,37] Therefore, transport of DXR by PITP–phospholipid complexes was responsible for the enhanced extracellular efflux of DXR. Moreover, because the cytotoxicity of DXR was increased by the suppression of PITP expression (Figure 4C), it seems likely that DXR transport by PITP–phospholipid complexes contributes to a decrease in the pharmacological effects of DXR. Because chols and PEG-modified phospholipids are not subject to intracellular transport by PITP,[18] PITP is unlikely to form a complex with either component, preventing an increase in the extracellular efflux of DXR *via* PITP complexes. PITP is involved in the transfer of lipid components between different membrane compartments and known as the conserved proteins in many cellular processes in various types of cells.[37] In the present study, we showed that

DXR formed a complex with PITP and phospholipids and that DXR underwent intracellular trafficking as a complex in cells exposed to encapsulated DXR. These findings suggest that PITP controls the efflux of encapsulated DXR and might provide a defensive mechanism against liposomal formulations in cancer cells. Taking these factors into consideration, to achieve potent pharmaceutical activities at low doses, the construction of liposomes lacking components that are subject to intracellular transport by PITP is effective for suppressing the extracellular efflux of DXR. In future studies we intend to evaluate the effects of other liposomal components, including cationic phospholipids, to provide further insight into the design of liposomes capable of enhancing the pharmacological properties of the encapsulated agents.

In conclusions, we determined the intracellular trafficking mechanism of PEG-modified phospholipids *in vitro*, and showed that PEG modification affects the intracellular trafficking of the modified molecules. We next showed that DXR increased the expression of PITP, ABCA1, and ABCB1, which are involved in the intracellular trafficking of phospholipids. DXR encapsulated into liposomes increased the extracellular efflux of liposomal phospholipids. We also found that the intracellular trafficking of DXR is controlled by PITP, which forms a complex with phospholipids and DXR in DXR-encapsulated liposomes. DXR-encapsulated PEG-modified liposomes have already been approved for clinical use in several countries and are expected to be promising anticancer agents. To date, there have been very few reports describing the intracellular trafficking of PEG-modified phospholipids or DXR. We believe that our findings might help with efforts to prepare novel formulations of DXR, including encapsulation in PEG-modified liposomes, to enhance the therapeutic effects and reduce unexpected toxicity of DXR.

■ ASSOCIATED CONTENT

Supporting Information

This material is available free of charge via the Internet at http://pubs.acs.org.

■ AUTHOR INFORMATION

Corresponding Author

*Telephone: +81-3-3700-9662. Fax: +81-3-3700-9662. E-mail: kumikato@nihs.go.jp.

Notes

The authors declare no competing financial interest.

■ ACKNOWLEDGMENTS

This work was supported in part by Health and Labour Sciences Research Grants from the Ministry of Health, Labour and Welfare of Japan, and by KAKENHI Grant Number 24590070 from the Japan Society for the Promotion of Science.

■ REFERENCES

(1) Adler-Moore, J.; Proffitt, R. T. AmBisome: liposomal formulation, structure, mechanism of action and pre-clinical experience. *J. Antimicrob. Chemother.* **2002**, *49*, 21–30.

(2) Wang, X.; Andersson, R.; Ding, J.; Norgren, L.; Bengmark, S. Reticuloendothelial system function following acute liver failure induced by 90% hepatectomy in the rat. *HPB Surg.* **1993**, *6*, 151–162.

(3) Allen, C.; Dos Santos, N.; Gallagher, R.; Chiu, G. N.; Shu, Y.; Li, W. M.; Johnstone, S. A.; Janoff, A. S.; Mayer, L. D.; Webb, M. S.; Bally, M. B. Controlling the physical behavior and biological performance of liposome formulations through use of surface grafted poly(ethylene glycol). *Biosci. Rep.* **2002**, *22*, 225–250.

(4) Immordino, M. L.; Dosio, F.; Cattel, L. Stealth liposomes: review of the basic science, rationale, and clinical applications, existing and potential. *Int. J. Nanomed.* **2006**, *1*, 297–315.

(5) Price, M. E.; Cornelius, R. M.; Brash, J. L. Protein adsorption to polyethylene glycol modified liposomes from fibrinogen solution and from plasma. *Biochim. Biophys. Acta* **2001**, *1512*, 191–205.

(6) Allen, T. M. Long-circulating (sterically stabilized) liposomes for targeted drug delivery. *Trends Pharmacol. Sci.* **1994**, *15*, 215–220.

(7) van Bochove, G. S.; Paulis, L. E.; Segers, D.; Mulder, W. J.; Krams, R.; Nicolay, K.; Strijkers, G. J. Contrast enhancement by differently sized paramagnetic MRI contrast agents in mice with two phenotypes of atherosclerotic plaque. *Contrast Media Mol. Imaging* **2011**, *6*, 35–45.

(8) Gabizon, A.; Shmeeda, H.; Barenholz, Y. Pharmacokinetics of pegylated liposomal Doxorubicin: review of animal and human studies. *Clin. Pharmacokinet.* **2003**, *42*, 419–436.

(9) Abraham, S. A.; Waterhouse, D. N.; Mayer, L. D.; Cullis, P. R.; Madden, T. D.; Bally, M. B. The liposomal formulation of doxorubicin. *Methods Enzymol.* **2005**, *391*, 71–97.

(10) Tirosh, O.; Barenholz, Y.; Katzhendler, J.; Priev, A. Hydration of polyethylene glycol-grafted liposomes. *Biophys. J.* **1998**, *74*, 1371–1379.

(11) Terada, T.; Iwai, M.; Kawakami, S.; Yamashita, F.; Hashida, M. Novel PEG-matrix metalloproteinase-2 cleavable peptide-lipid containing galactosylated liposomes for hepatocellular carcinoma-selective targeting. *J. Controlled Release* **2006**, *111*, 333–342.

(12) Hatakeyama, H.; Akita, H.; Ishida, E.; Hashimoto, K.; Kobayashi, H.; Aoki, T.; Yasuda, J.; Obata, K.; Kikuchi, H.; Ishida, T.; Kiwada, H.; Harashima, H. Tumor targeting of doxorubicin by anti-MT1-MMP antibody-modified PEG liposomes. *Int. J. Pharm.* **2007**, *342*, 194–200.

(13) Sakai-Kato, K.; Ishikura, K.; Oshima, Y.; Tada, M.; Suzuki, T.; Ishii-Watabe, A.; Yamaguchi, T.; Nishiyama, N.; Kataoka, K.; Kawanishi, T.; Okuda, H. Evaluation of intracellular trafficking and clearance from HeLa cells of doxorubicin-bound block copolymers. *Int. J. Pharm.* **2012**, *423*, 401–409.

(14) Fardel, O.; Lecureur, V.; Daval, S.; Corlu, A.; Guillouzo, A. Up-regulation of P-glycoprotein expression in rat liver cells by acute doxorubicin treatment. *Eur. J. Biochem.* **1997**, *246*, 186–192.

(15) Mercier, C.; Declèves, X.; Masseguin, C.; Fragner, P.; Tardy, M.; Roux, F.; Gabrion, J.; Scherrmann, J. M. P-glycoprotein (ABCB1) but not multidrug resistance-associated protein 1 (ABCC1) is induced by doxorubicin in primary cultures of rat astrocytes. *J. Neurochem.* **2003**, *87*, 820–830.

(16) Shukla, A.; Hillegass, J. M.; MacPherson, M. B.; Beuschel, S. L.; Vacek, P. M.; Pass, H. I.; Carbone, M.; Testa, J. R.; Mossman, B. T. Blocking of ERK1 and ERK2 sensitizes human mesothelioma cells to doxorubicin. *Mol. Cancer* **2010**, *9*, 314.

(17) Bao, L.; Haque, A.; Jackson, K.; Hazari, S.; Moroz, K.; Jetly, R.; Dash, S. Increased expression of P-glycoprotein is associated with doxorubicin chemoresistance in the metastatic 4T1 breast cancer model. *Am. J. Pathol.* **2011**, *178*, 838–852.

(18) Un, K.; Sakai-Kato, K.; Oshima, Y.; Kawanishi, T.; Okuda, H. Intracellular trafficking mechanism, from intracellular uptake to extracellular efflux, for phospholipid/cholesterol liposomes. *Biomaterials* **2012**, *33*, 8131–8141.

(19) Bangham, A. D.; Standish, M. M.; Watkins, J. C. Diffusion of univalent ions across the lamellae of swollen phospholipids. *J. Mol. Biol.* **1965**, *13*, 238–252.

(20) Fritze, A.; Hens, F.; Kimpfler, A.; Schubert, R.; Peschka-Süss, R. Remote loading of doxorubicin into liposomes driven by a transmembrane phosphate gradient. *Biochim. Biophys. Acta* **2006**, *1758*, 1633–1640.

(21) Rejman, J.; Bragonzi, A.; Conese, M. Role of clathrin- and caveolae-mediated endocytosis in gene transfer mediated by lipo- and polyplexes. *Mol. Ther.* **2005**, *12*, 468–474.

(22) Perez, A. P.; Cosaka, M. L.; Romero, E. L.; Morilla, M. J. Uptake and intracellular traffic of siRNA dendriplexes in glioblastoma cells and macrophages. *Int. J. Nanomed.* **2011**, *6*, 2715−2728.
(23) Johansson, M.; Bocher, V.; Lehto, M.; Chinetti, G.; Kuismanen, E.; Ehnholm, C.; Staels, B.; Olkkonen, V. M. The two variants of oxysterol binding protein-related protein-1 display different tissue expression patterns, have different intracellular localization, and are functionally distinct. *Mol. Biol. Cell* **2003**, *14*, 903−915.
(24) Hölttä-Vuori, M.; Alpy, F.; Tanhuanpää, K.; Jokitalo, E.; Mutka, A. L.; Ikonen, E. MLN64 is involved in actin-mediated dynamics of late endocytic organelles. *Mol. Biol. Cell* **2005**, *16*, 3873−86.
(25) Koivusalo, M.; Jansen, M.; Somerharju, P.; Ikonen, E. Endocytic trafficking of sphingomyelin depends on its acyl chain length. *Mol. Biol. Cell* **2007**, *18*, 5113−5123.
(26) Xu, S.; Benoff, B.; Liou, H. L.; Lobel, P.; Stock, A. M. Structural basis of sterol binding by NPC2, a lysosomal protein deficient in Niemann-Pick type C2 disease. *J. Biol. Chem.* **2007**, *282*, 23525−23531.
(27) Hanada, K.; Kumagai, K.; Tomishige, N.; Kawano, M. CERT and intracellular trafficking of ceramide. *Biochim. Biophys. Acta* **2007**, *1771*, 644−653.
(28) Jensen, D.; Schekman, R. COPII-mediated vesicle formation at a glance. *J. Cell Sci.* **2011**, *124*, 1−4.
(29) Hsuan, J.; Cockcroft, S. The PITP family of phosphatidylinositol transfer proteins. *Genome Biol.* **2001**, *2*, 1−8.
(30) Hynynen, R.; Suchanek, M.; Spandl, J.; Bäck, N.; Thiele, C.; Olkkonen, V. M. OSBP-related protein 2 is a sterol receptor on lipid droplets that regulates the metabolism of neutral lipids. *J. Lipid Res.* **2009**, *50*, 1305−1315.
(31) Kimura, Y.; Morita, S. Y.; Matsuo, M.; Ueda, K. Mechanism of multidrug recognition by MDR1/ABCB1. *Cancer Sci.* **2007**, *98*, 1303−1310.
(32) Rose, P. G. Pegylated liposomal doxorubicin: optimizing the dosing schedule in ovarian cancer. *Oncologist* **2005**, *10*, 205−214.
(33) Smit, J. W.; Duin, E.; Steen, H.; Oosting, R.; Roggeveld, J.; Meijer, D. K. Interactions between P-glycoprotein substrates and other cationic drugs at the hepatic excretory level. *Br. J. Pharmacol.* **1998**, *123*, 361−370.
(34) Kondratov, R. V.; Komarov, P. G.; Becker, Y.; Ewenson, A.; Gudkov, A. V. Small molecules that dramatically alter multidrug resistance phenotype by modulating the substrate specificity of P-glycoprotein. *Proc. Natl. Acad. Sci. U.S.A.* **2001**, *98*, 14078−14083.
(35) Shen, F.; Chu, S.; Bence, A. K.; Bailey, B.; Xue, X.; Erickson, P. A.; Montrose, M. H.; Beck, W. T.; Erickson, L. C. Quantitation of doxorubicin uptake, efflux, and modulation of multidrug resistance (MDR) in MDR human cancer cells. *J. Pharmacol. Exp. Ther.* **2008**, *324*, 95−102.
(36) Ségui, B.; Allen-Baume, V.; Cockcroft, S. Phosphatidylinositol transfer protein beta displays minimal sphingomyelin transfer activity and is not required for biosynthesis and trafficking of sphingomyelin. *Biochem. J.* **2002**, *366*, 23−34.
(37) Garner, K.; Hunt, A. N.; Koster, G.; Somerharju, P.; Groves, E.; Li, M.; Raghu, P.; Holic, R.; Cockcroft, S. Phosphatidylinositol transfer protein, cytoplasmic 1 (PITPNC1) binds and transfers phosphatidic acid. *J. Biol. Chem.* **2012**, *287*, 32263−32276.
(38) Li, X.; Ding, L.; Xu, Y.; Wang, Y.; Ping, Q. Targeted delivery of doxorubicin using stealth liposomes modified with transferrin. *Int. J. Pharm.* **2009**, *373*, 116−123.
(39) Jung, S. H.; Jung, S. H.; Seong, H.; Cho, S. H.; Jeong, K. S.; Shin, B. C. Polyethylene glycol-complexed cationic liposome for enhanced cellular uptake and anticancer activity. *Int. J. Pharm.* **2009**, *382*, 254−261.

Biomaterials 35 (2014) 1347–1358

Contents lists available at ScienceDirect

Biomaterials

journal homepage: www.elsevier.com/locate/biomaterials

Leading opinion

Elucidating the molecular mechanism for the intracellular trafficking and fate of block copolymer micelles and their components

Kumiko Sakai-Kato [a,*], Keita Un [a], Kunie Nanjo [a], Nobuhiro Nishiyama [b], Hiroyuki Kusuhara [c], Kazunori Kataoka [d,e], Toru Kawanishi [f], Yukihiro Goda [a], Haruhiro Okuda [f]

[a] Division of Drugs, National Institute of Health Sciences, 1-18-1 Kamiyoga, Setagaya-ku, Tokyo 158-8501, Japan
[b] Polymer Chemistry Division, Chemical Resources Laboratory, Tokyo Institute of Technology, R1-11, 4259 Nagatsuda, Midori, Yokohama 226-8503, Japan
[c] Laboratory of Molecular Pharmacokinetics, Graduate School of Pharmaceutical Sciences, The University of Tokyo, 7-3-1 Hongo, Bunkyo, Tokyo 113-0033, Japan
[d] Center for Disease Biology and Integrative Medicine, Graduate School of Medicine, The University of Tokyo, 7-3-1 Hongo, Bunkyo, Tokyo 113-0033, Japan
[e] Department of Materials Engineering, Graduate School of Engineering, The University of Tokyo, 7-3-1 Hongo, Bunkyo, Tokyo 113-8656, Japan
[f] National Institute of Health Sciences, 1-18-1 Kamiyoga, Setagaya-ku, Tokyo 158-8501, Japan

ARTICLE INFO

Article history:
Received 17 October 2013
Accepted 8 November 2013
Available online 2 December 2013

Keywords:
Block copolymer micelles
Intracellular trafficking
Intermembrane transport
NPC1
ORP2
ABCB1

ABSTRACT

Block copolymer micelles have shown promise for the intracellular delivery of chemotherapeutic agents, proteins, and nucleic acids. Understanding the mechanism of their intracellular trafficking and fate, including the extracellular efflux of the polymers, will help improve their efficacy and minimize their safety risks. In this Leading Opinion paper, we discuss the molecular mechanism of block copolymer micelle trafficking, from intracellular uptake to extracellular efflux, on the basis of studies with HeLa cells. By using FRET (fluorescence resonance energy transfer) with confocal microscopy, we found that, following their intracellular transport via endocytosis, the micelles dissociated into their polymeric components in late endosomes and/or lysosomes. Furthermore, we confirmed that the intrinsic proteins NPC1 and ORP2 are involved in the intermembrane transfer of polymers from the endosome to the plasma membrane via the ER (endoplasmic reticulum) by using knockdown experiments with siRNAs. After the polymers were transported to the plasma membrane with the aid of ORP2, they were extruded into the cell medium via ABC transporter, ABCB1. Experiments with ABCB1-expressing vesicles indicated that the polymer itself, and not the fluorescent compounds, was recognized by the transporter. These findings, and the analysis of related mechanisms, provide valuable information that should help minimize the potential risks associated with the intracellular accumulation of block copolymer micelles and to improve their therapeutic efficacy.

1. Introduction

Drug delivery systems that use nanometer-sized carriers show promise for the targeted transfer of chemotherapeutic agents, proteins, and nucleic acids to tissues or organs. Nanomaterials have been extensively studied as drug carriers, and some formulations for cancer treatment have been applied clinically [1–3]. Block copolymer micelles have recently received considerable attention as targetable carrier systems [4–7]. The formulation of block copolymer micelles can alter the pharmacokinetic characteristics such as the volume of distribution, clearance, half-life, and tissue distribution of the active substances included [8–10]. Moreover, finely tuning the design of the block copolymers can increase their longevity in the bloodstream and allow the controlled release of the drugs, which consequently improves the pharmacodynamics of the drugs and/or avoids systemic toxicity.

The development of these drug carriers for the cellular uptake of therapeutic proteins and nucleic acids is of particular interest. Because nucleic acids, proteins, and peptides are not taken up into cells via passive diffusion, their intracellular uptake by nanocarriers is a key to targeting the delivery of these compounds at the cellular or organelle level. Specifically, the incorporation of these compounds into nanocarriers will improve the efficiency of their intracellular uptake or delivery to specific organelle, thereby ensuring their therapeutic effects. Furthermore, clarifying the intracellular trafficking mechanisms may also facilitate the

* Corresponding author. Tel./fax: +81 3 3700 9662.
E-mail address: kumikato@nihs.go.jp (K. Sakai-Kato).

0142-9612/$ – see front matter © 2013 Elsevier Ltd. All rights reserved.
http://dx.doi.org/10.1016/j.biomaterials.2013.11.027

discovery of new drug delivery strategies, such as targeting to specific cell organelles. Thus, to improve the efficiency of the intracellular uptake of these compounds, it is essential to understand the detailed mechanism of their trafficking including the fate of the micelles and their component polymers after their uptake via endocytosis. To this end, the use of covalently bound fluorescent reagents as probes has gradually shed light on the internalization pathways and intracellular localizations of polymeric nanoparticulate carriers [11–13].

In parallel, the safety of these carriers must be investigated. To ensure that these materials are safe, it is essential to know whether the components of the carriers are accumulated inside the cell or undergo sequestration (i.e., metabolism or efflux). The potential long-term effects of these novel polymers when used as nanosized particles have not yet been determined. To address this issue, we investigated the intracellular fate of polymer micelles conjugated with doxorubicin (Dox) in HeLa cells [14]. We demonstrated that Dox is endocytosed and localized to the endoplasmic reticulum, and that an ABC transporter, ABCB1, is involved in the efflux of the polymer from these cells. However, many factors remain unknown, for example, where do the micelles dissociate into their constituent polymers after internalization? What are the molecular mechanisms involved in trafficking to each organelle and in the efflux of polymers or micelles? Moreover, the trafficking phenomenon we found previously was limited to the case of Dox-conjugated polymers. Questions remain regarding the trafficking of other block copolymers, for example, those conjugated with different compounds or those with different poly(ethylene glycol) (PEG) lengths.

In the present study, we constructed three micelles by using three block copolymers (doxorubicin, Nile Red, and DBD (4-(*N*,*N*-dimethylsulfamoyl)-2,1,3-benzoxadiazole)) with different poly(ethylene glycol) (PEG) lengths (Mw 5000 or 12,000), detailed descriptions of which can be found in Section 3.1. To investigate the structural integrity of the micelles inside the cells, fluorescence resonance energy transfer (FRET) micelles were also constructed by using two types of polymers, that is, polymers with covalently bound Nile Red and polymers with covalently bound DBD. The trafficking of the micelles and their components, from intracellular uptake to extracellular efflux, was evaluated and the intrinsic molecules involved in the trafficking process were identified.

2. Materials and methods

2.1. Materials

Poly(ethylene glycol)–poly(aspartate) (PEG–P(Asp)) block copolymers with conjugated Dox were synthesized by Nippon Kayaku Co., Ltd. (Tokyo, Japan) [15]. Dextran (Dextran Texas Red, Molecular weight 10,000), polystyrene particles (FluoSphere Red, average particle size; 40.1 nm), Dulbecco's modified Eagle's Medium (DMEM), RPMI-1640, penicillin/streptomycin, and Opti-MEM I were purchased from Life Technologies (Brooklyn, NY, USA). Fetal bovine serum (FBS) was obtained from Nichirei Biosciences (Tokyo, Japan). Fluorescently labeled amorphous silica particles (Sicastar RedF, average particle size; 45.5 nm) were obtained from Micromod Partikeltechnologie (Rostock, Germany). Isolated mammalian cell membranes containing human ABCB1, for vesicle transport assays, (SB-MDR1-K-VT) were purchased from SOLVO Biotechnology (Hungary). All chemicals used in this study were of the highest purity available. HeLa cells (Health Science Research Resources Bank, Osaka, Japan) were cultured in DMEM. The medium was supplemented with 10% FBS, 100 U/mL penicillin/streptomycin. Cells were grown in a humidified incubator at 37 °C/5% CO_2.

2.2. Synthesis of the DBD-conjugated polymer and Nile Red-conjugated polymer

Poly(ethylene glycol)–poly(aspartate) block copolymer (PEG–P(Asp)) was obtained as described previously [15]. The degree of polymerization of PEG–P(Asp) was determined to be 35–45 by neutralization titration (Supplementary Fig. 1-1).

For the synthesis of DBD-conjugated polymer, PEG–P(Asp) (100 mg) and dimethylaminopyridine (23 mg, 0.8 equiv. for COOH) were dissolved in DMF (1.5 mL) and then DBD-ED (13 mg, 0.2 equiv.) and 4-phenyl-1-butanol (25 μL, 0.7 equiv.) were added. Diisopropylcarbodiimide (36 μL, 1.0 equiv.) was added to the solution and stirred at room temperature for 5 h. Diisopropylcarbodiimide (36 μL, 1.0 equiv.) was added again and the solution was stirred for 18 h. The reaction mixture was then dropped into a mixture of ethyl acetate and hexane (1:3). The resulting precipitate was filtered, washed with the mixture of ethyl acetate and hexane (1:3), and dried under vacuum to obtain the DBD-conjugated polymer (99 mg) as a powder. ^{1}H NMR spectra in DMSO-d_6 and the assignment are shown in Supplementary Fig. 1-2.

For the synthesis of the Nile Red-conjugated polymer, PEG–P(Asp) (100 mg) and dimethylaminopyridine (28 mg, 1.0 equiv.) were dissolved in DMF (1.5 mL) and then Nile-Red (8.8 mg, 0.1 equiv.) and 4-phenyl-1-butanol (36 μL, 1.0 equiv.) were added. Diisopropylcarbodiimide (36 μL, 1.0 equiv.) was added to the solution, which was then stirred at room temperature for 18 h. The reaction mixture was dropped into a mixture of ethyl acetate and hexane (1:3). The resulting precipitate was filtered, washed with the mixture of ethyl acetate and hexane (1:3), and dried under vacuum to obtain the Nile Red-conjugated polymer (109 mg) as a powder. ^{1}H NMR spectra in DMSO-d_6 and the assignment are shown in Supplementary Fig. 1-3.

2.3. Physicochemical properties of block copolymer micelles

The particle size and polydispersity index (PDI) of the block copolymer micelles were determined with a Zetasizer Nano ZS instrument (Malvern Instruments, Worcestershire, UK).

2.4. Evaluation of the intracellular trafficking of block copolymer micelles

To quantify the intracellular uptake of the polymers, we used a final polymer concentration of 50 μg/mL in this study. HeLa cells (5×10^4) were seeded onto 6-well plates in medium containing 10% FBS and 100 U/mL penicillin/streptomycin. After incubation for 24 h at 37 °C/5% CO_2, the cells were exposed to 50 μg/mL micelles in culture medium. After incubation for pre-determined durations, the incubation medium was replaced with Hanks' balanced salt solution (HBSS). The cells were trypsinized with 0.25% trypsin–ethylenediamine tetraacetic acid (EDTA) (Life Technologies), washed with HBSS three times, and suspended in lysis buffer (1.0% Triton X-100 in HBSS). The cell suspension was then shaken and centrifuged (15,000× *g*, 4 °C, 10 min). The fluorescence intensity of the resultant supernatant was measured on a fluorescence spectrophotometer (F-7000; Hitachi High-Technologies, Tokyo, Japan) using 440 nm excitation and 580 nm emission for DBD-conjugated polymers, 580 nm excitation and 640 nm emission for Nile Red-conjugated polymers, and 470 nm excitation and 590 nm emission for Dox-conjugated polymers. The fluorescence intensity was normalized with respect to the protein content of the cells. The protein concentration was determined by using a Protein Assay Kit (Bio-Rad Laboratories, Hercules, CA, USA).

2.5. Confocal microscopy

To observe the colocalization of block copolymer micelles with the intracellular compartment, specific intracellular compartment components were labeled by using fluorescent dyes. All dyes for confocal microscopy were purchased from Life Technologies and used in accordance with the manufacturer's instructions. Endosomes were labeled with transferrin conjugated to Alexa Fluor 488 or Alexa Fluor 594, and lysosomes were labeled with LysoTracker Green DND-26 or LysoTracker Red DND-99. The ER was labeled with ER-Tracker Green or ER-Tracker Red, and the Golgi apparatus was labeled with Bodipy-FL C5-ceramide or Bodipy-TR C5-ceramide complexed to BSA. Confocal microscopy was performed as previously described [14]. Briefly, cells (1.0×10^5) were plated on 35-mm glass-bottom dishes coated with poly-L-lysine (Matsunami Glass, Osaka, Japan) in medium containing 10% FBS and 100 U/mL penicillin/streptomycin. After incubation for 24 h, cells were exposed to 50 μg/mL micelles in culture medium. At a pre-determined time after addition of the micelles, cells were washed and kept in HBSS for imaging with a confocal microscope (Carl Zeiss LSM 510; Carl Zeiss Microscopy GmbH, Germany). Pseudocolor luminescent images were captured using LSM Image Browser (Carl Zeiss Microscopy GmbH, Germany).

An FRET experiment was performed using FRET micelles composed of DBD-conjugated polymers and Nile Red polymers (9:1, w:w). Cells were exposed to 50 μg/mL FRET micelles in culture medium. Two hours after addition of the micelles, cells were washed and kept in medium without micelles and then imaged with a confocal microscope at 2, 10, and 24 h after addition of the micelles.

2.6. Endocytosis inhibition and Golgi destruction

To investigate the mechanism of endocytosis of the prepared micelles, 10 μg/mL chlorpromazine (a clathrin-mediated endocytosis inhibitor), 150 μM genistein or 2.0 mM methyl-β-cyclodextrin (MβCD) (caveolae-mediated endocytosis inhibitors), or 50 μM 5-(N-ethyl-N-isopropyl) amiloride (a macropinocytosis inhibitor) were used [16,17]. Each endocytosis inhibitor was added to the culture medium 30 min before the addition of the micelles. To inhibit ER-to-Golgi transfer, to investigate whether ER-to-Golgi transfer is involved in the intracellular trafficking of micelles or polymers, cells were incubated in medium containing 1 μg/mL brefeldin A 30 min before the addition of the micelles [18].

2.7. Small interfering RNA (siRNA) transfer

To clarify which intrinsic proteins are involved in the intracellular trafficking and efflux of the polymers, the expression of specific proteins was down-regulated by

using siRNA. Stealth RNAi oligonucleotides (25-mer, Life Technologies), which unlike conventional siRNAs can reduce the cytotoxic interferon response [19], were obtained from Life Technologies. The siRNA sequences used in this study are shown in Table 1. As a negative control, the Stealth RNAi High GC Negative Control Duplex (Life Technologies) was used [14]. The Stealth RNAi oligonucleotides were transfected into cells by using Lipofectamine RNAiMAX (Life Technologies) according to the manufacturer's protocols. Briefly, the cells were incubated for 24 h. Each siRNA was then added, and the cells were incubated for a further 48 h, at which time the micelles (50 μg/mL) were added. Western blotting was used to confirm the down-regulation of each protein as described previously [14]. After the cells were incubated with the micelles, the culture medium was replaced with HBSS. Cells were trypsinized and lysed to quantify the intracellular amount of polymer as described above (Section 2.3).

2.8. Transport experiment

To investigate ATP-dependent transport, mammalian cell membrane vesicles expressing ABCB1 were used according to the manufacturer's instructions. Suspensions of vesicles expressing ABCB1, and control vesicles without ABCB1 (50 μL each), were plated on a 96-well plate. Samples (0.75 μL) at the indicated concentration and reaction buffer (25 μL) were added to each well, and the plates were incubated at 37 °C for 5 min. After washing by centrifugation (1500× *g*, 5 min, 4 °C), the fluorescence intensity of the polymers after intravesicular transport was measured using a fluorescence spectrophotometer as described in Section 2.3. The fluorescence intensity of intravesicular polymers incubated with MgATP was subtracted from that of polymers incubated without MgATP.

2.9. Statistical analyses

Results are presented as the mean ± SD of more than three experiments. Analysis of variance was used to test the statistical significance of the differences among groups. Two-group comparisons were performed with a Student's *t*-test. Multiple comparisons between control and test groups were performed with a Dunnett's test.

3. Results

3.1. Chemical structures of block copolymers and physicochemical properties

We used three different kinds of micelles formed from Dox-conjugated, DBD-conjugated, and Nile Red-conjugated PEG–P(Asp) block copolymers, respectively (Supplementary Fig. 1), hereinafter referred to as Dox-conjugated polymers, DBD-conjugated polymers, and Nile Red-conjugated polymers, respectively. Dox-conjugated polymers consisted of PEG (M_w ~5000) and P(Asp) (polymerization degree, 30) with partially conjugated doxorubicin (ca. 45%) to the side chain of the P(Asp) [15]. DBD-conjugated polymers consist of PEG (M_w ~12,000) and P(Asp) (polymerization degree, 35–45), with partially conjugated DBD (ca. 10%) and 4-phenyl-1-butanol (ca. 43%) to increase the hydrophobicity to the side chain of the P(Asp). Nile Red-conjugated polymers consist of PEG (M_w ~12,000) and P(Asp) (polymerization degree, 35–45) with partially conjugated Nile Red (ca. 10%) and 4-phenyl-1-butanol (ca. 53%) to increase the hydrophobicity to the side chain of the P(Asp). When these block copolymers were dissolved in aqueous medium, they spontaneously formed micelles with hydrophobic cores. We constructed FRET micelles by mixing DBD-conjugated polymers with Nile Red-conjugated polymers. The particle sizes of the resultant micelles (~30 nm) are shown in Table 2.

Table 2
Particle sizes and PDI of block copolymer micelles used in this study.

	Particle size	PDI
DBD-conjugated polymer micelles	31.7 ± 0.11	0.180 ± 0.011
NR-conjugated polymer micelles	31.4 ± 0.67	0.184 ± 0.006
Dox-conjugated polymer micelles	32.3 ± 0.19	0.180 ± 0.014
DBD:NR (9:1)-conjugated polymer micelles	32.4 ± 0.18	0.198 ± 0.005

Each value represents the mean ± S.D. ($n = 3$).

3.2. Endocytosis of block copolymers

To investigate the intracellular transport mechanisms of the micelles and their components, we used confocal microscopy to observe the intracellular trafficking of fluorescent micelles composed of Dox-, Nile Red- or DBD-conjugated polymers. All three of the different types of fluorescent micelle colocalized with the endosomes after 1 h in HeLa cells (Fig. 1A). At 2 h-post-incubation, most of the micelles colocalized with the lysosomes although some were distributed outside the vesicles (Fig. 1B).

The use of endocytosis inhibitors to clarify the endocytosis mechanism demonstrated that the internalized amounts of fluorescent micelles in HeLa cells were significantly suppressed at 2, 24 and 48 h in the presence of chlorpromazine (Fig. 2). Genistein and MβCD also inhibited the intracellular uptake of all of the micelles at 24 and 48 h, although the extent of inhibition was less in the case of genistein and MβCD compared with that of chlorpromazine. These results indicate that the intracellular uptake of the micelles proceeded mainly through clathrin-mediated endocytosis. Caveolae-mediated endocytosis also contributed to the uptake over time.

3.3. Dissociation of micelles into polymers in HeLa cells

We then attempted to identify the intracellular location where the block copolymer micelles dissociate into polymers after internalization. We constructed an FRET system to track the structural integrity of the micelles once they were internalized into the HeLa cells. FRET is a distance-dependent process in which excitation energy is absorbed by a molecular fluorophore (the donor) and then transferred to a nearby fluorophore (the acceptor). It is a highly sensitive technique for investigating biological phenomena that produce changes in molecular proximity [20,21]. We used micelles consisting of DBD-conjugated polymers and Nile Red-conjugated polymers (9:1, w/w; Fig. 3A). The mixing ratio of 9:1 of DBD-:Nile Red-conjugated polymers resulted in the formation of

Table 1
The siRNA sequences used in this study.

Target gene	Sense strand	Antisense strand
MLN64	5′-GCUGA AGGAU UAAAC AAUGA CUUCA-3′	5′-UGAAG UCAUU GUUUA AUCCU UCAGC-3′
ORP1	5′-GCACC UCUGA GGAGU UGGAU GAAAU-3′	5′-AUUUC AUCCA ACUCC UCAGA GGUGC-3′
NPC1	5′-CCCUC GUCCU GGAUC GACGA UUAUU-3′	5′-AAUAA UCGUC GAUCC AGGAC GAGGG-3′
CERT	5′-ACGUG AGAAG UUGGC UGAAA UGGAA-3′	5′-UUCCA UUUCA GCCAA CUUCU CACGU-3′
Sec31A	5′-CCAGG CCAAU AAGCU GGGUG UCUAA-3′	5′-UUAGA CACCC AGCUU AUUGG CCUGG-3′
ORP2	5′-GAGAG GAGAG GUGAC CACCU GAGAA-3′	5′-UUCUC AGGUG GUCAC CUCUC CUCUC-3′
PITP	5′-GGAUA UUUAC AAACU UCCAU CGCCA-3′	5′-UGGCG AUGGA AGUUU GUAAA UAUCC-3′
ABCA1	5′-UUUAG AUGCU GGACA CUGCC AAGGC-3′	5′-GCCUU GGCAG UGUCC AGCAU CUAAA-3′
ABCB1	5′-UCCCG UAGAA ACCUU ACAUU UAUGG-3′	5′-CCAUA AAUGU AAGGU UUCUA CGGGA-3′
ABCC1	5′-CCGGU CUAUU CCCAU UUCAA CGAGA-3′	5′-UCUCG UUGAA AUGGG AAUAG ACCGG-3′
ABCG1	5′-UCUCG CUGAU GAAAG GGCUC GCUCA-3′	5′-UGAGC GAGCC CUUUC AUCAG CGAGA-3′
Snap-25	5′-CAUGG AGAAG GCUGA UUCCA ACAAA-3′	5′-UUUGU UGGAA UCAGC CUUCU CCAUG-3′

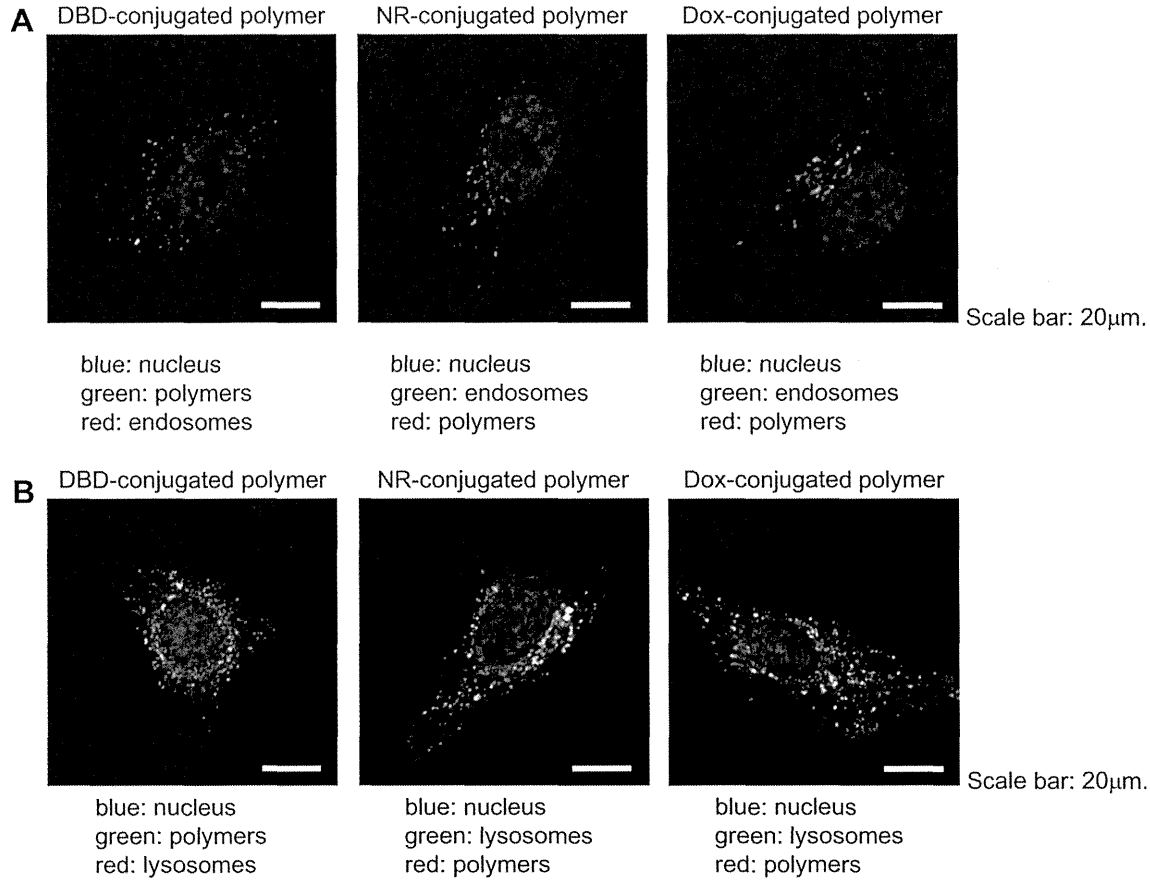

Fig. 1. (A) Confocal images showing the intracellular transport of micelles at 1 h after the addition of the micelles to HeLa cells. The endosomes are labeled with Alexa Fluor-conjugated transferrin. Scale bars = 20 μm. (B) Confocal images showing the intracellular transport of micelles at 2 h after the addition of the micelles to HeLa cells. The lysosomes are labeled with LysoTracker Red or Green. Scale bars = 20 μm.

block copolymer micelles with the most effective FRET efficiency. At 2 h after the addition of the micelles, we washed the cells with fresh medium to stop any further entry of micelles into the HeLa cells, whereupon only red (in web version) fluorescence was observed in the vesicular structure (Fig. 3B). Together with the result of the cellular uptake experiments, these results show that the block copolymers mostly maintain their micellar structure for at least 2 h after their internalization. Confocal microscopy images were taken at time intervals up to 24 h after the addition of the micelles. The fluorescence of the vesicular structures changed to yellow (in web version) after 10 h and then to green (in web version) after 24 h suggesting that the micelles gradually dissociated into polymers upon localization in the endosomes and/or lysosomes (Fig. 3B).

3.4. Intracellular trafficking of block copolymers

Using confocal microscopy, we further examined the intracellular trafficking of block copolymers with conjugated fluorescent compounds after their internalization. The fluorescence of all three polymers was colocalized to the ER, but not to the Golgi apparatus of the HeLa cells (Fig. 4). This is consistent with our previous study showing that Dox-bound micelles colocalize to the ER but not to the Golgi apparatus [14].

3.5. Molecular mechanisms of intracellular trafficking from endosomes/lysosomes to the cytoplasm and ER

In the case of cholesterol, there is some evidence for a direct pathway from endosomes to the ER [22,23]. We, therefore, investigated whether the molecular mechanisms involved in the transport of cholesterol or other lipid analogs are also implicated in the intracellular trafficking of block copolymers. To elucidate the molecular mechanisms of block copolymer transport in HeLa cells, we used siRNAs to down-regulate the expression of specific lipid transport proteins. We hypothesized that the suppression of specific intracellular transport processes would decrease the extracellular efflux of the block copolymers, thereby leading to an increase in the intracellular amounts of each polymer. Fig. 5A shows the intracellular components and the typical lipid transport proteins we investigated. At 48 h after transfection with stealth RNAis, the expression of each protein was down-regulated in HeLa cells, which allowed us to investigate the role of these proteins in polymer transport (Supplementary Fig. 2). Initially, we investigated lipid transport proteins that are involved in intracellular trafficking from endosomes/lysosomes to other compartments, including the ER. These proteins included metastatic lymph-node gene 64 protein (MLN64) [24], oxysterol-binding protein-related protein 1 (ORP1) [25], and Niemann–Pick C1 protein (NPC1) [26,27]. Fig. 5B shows the amounts of intracellular polymer increased upon suppression of NPC1 expression. Confocal microscopy also revealed that the transport of polymers from endosomes or lysosomes to the ER was suppressed when NPC1 expression was knocked-down (Fig. 5C). These results suggest that NPC1 partially controls the intracellular trafficking of the polymers from the endosomes or lysosomes to the ER. On the other hand, they also indicate that MLN64 and ORP1, which are sterol-binding proteins that are involved in organizing late endosomal membrane trafficking, are not involved in the trafficking of these polymers. To determine

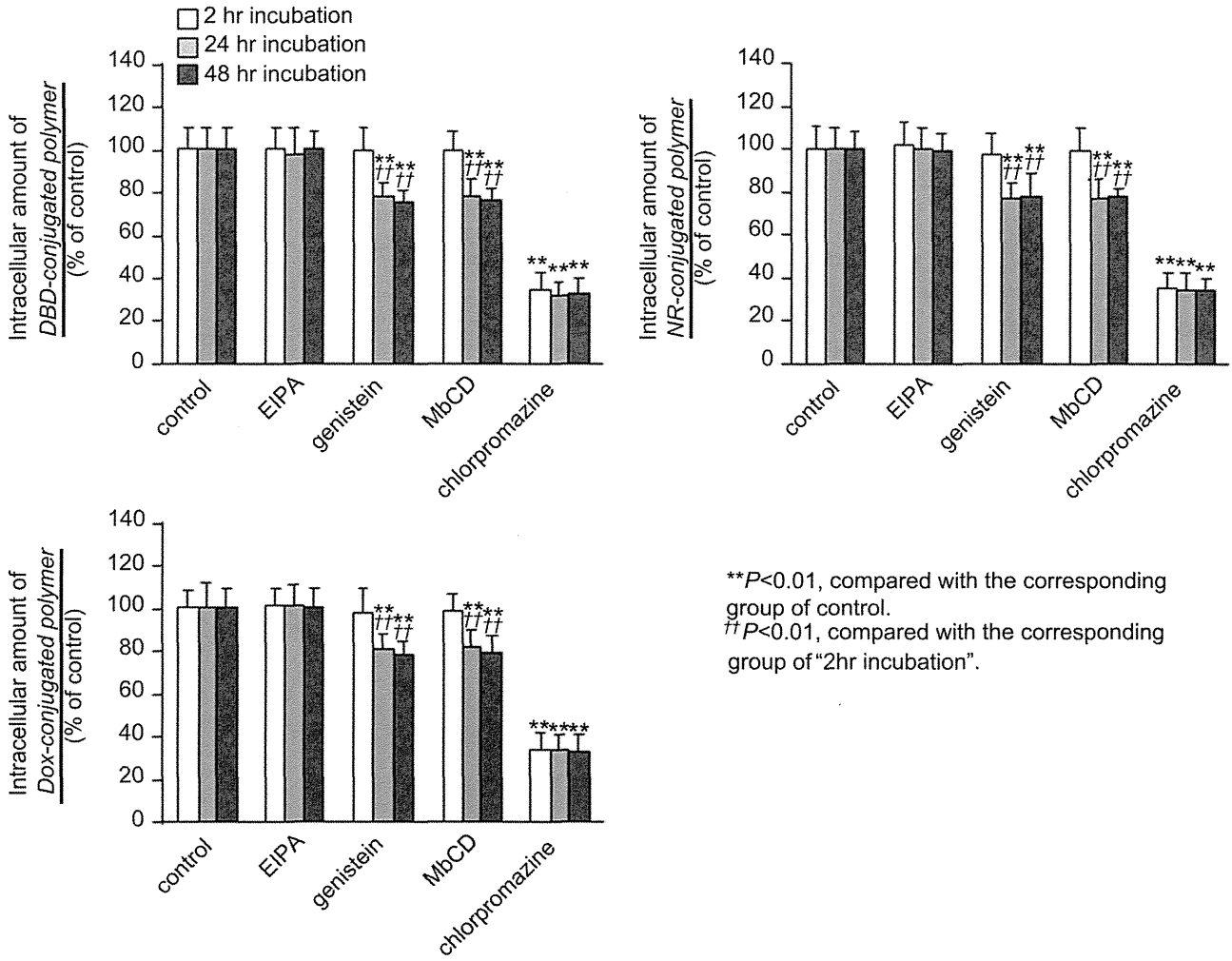

Fig. 2. The effect of endocytosis inhibitors on the intracellular amounts of polymers. The intracellular transport of micelles was evaluated at 2, 24, and 48 h after the addition of micelles to HeLa cells. Each endocytosis inhibitor was added to the cells 30 min before the addition of the micelles. $^{**}P < 0.01$ compared with the corresponding control group. $^{††}P < 0.01$, compared with the corresponding group of "cells incubated for 2 h". Each value represents the mean ± SD ($n = 6$).

whether the absence of NPC1 also leads to increased retention of other polymers or nanoparticles that are internalized via endocytosis, we tested dextran, polystyrene nanoparticle, and silica nanoparticle. We found that the amounts of intracellular dextran, polystyrene nanoparticles, and silica nanoparticles were not affected by the suppression of NPC1 expression (Supplementary Fig. 3). These results thus show that NPC1 is not involved in trafficking of all polymers or nanoparticles from NPC1-positive late endosomes.

ER-to-Golgi transport is a major trafficking route for lipid molecules. Therefore, we investigated the involvement of ER-to-Golgi transport in the intracellular trafficking of block copolymers by examining whether trafficking was affected if ER-to-Golgi transport-related proteins were inhibited. We selected CERT, a known ceramide-transfer protein [28,29], and sec31A, a component of COPII that is required for the budding of vesicles from the ER [30,31] (Fig. 5A) for this assessment. The intracellular amounts of polymer were not affected by CERT or sec31A knockdown (Supplementary Fig. 4A), nor were they affected by the presence of brefeldin A, an inhibitor of the transport pathway from the ER to the Golgi apparatus [18] (Supplementary Fig. 4B). These results suggest that the ER-to-Golgi transport system is not involved in polymer trafficking, which is consistent with our results indicating that the polymers did not localize to the Golgi apparatus (Fig. 4B).

3.6. Molecular mechanism for the extracellular efflux of polymers

To investigate the transport of polymers to the plasma membrane, we examined oxysterol-binding protein-related protein 2 (ORP2) [32–34] and phosphatidylinositol transfer protein (PITP) [35–37]. These proteins are both involved in the intracellular transport of lipid molecules (Fig. 5A). Knockdown experiments using siRNAs against each protein revealed that the intracellular amounts of all three polymers did not change with the suppression of PITP, but increased upon the suppression of ORP2, a molecule involved in the trafficking of endogenous cholesterol (Fig. 6). On the other hand, the intracellular amounts of dextran, silica nanoparticles, and polystyrene nanoparticles were not affected by the suppression of ORP2 expression. (Supplementary Fig. 5A).

We previously reported that ABCB1, a member of the ATP-binding cassette (ABC) transporter family, is involved in the efflux of Dox-conjugated block copolymers [14]. ABCB1, also known as MDR-1 or P-gp, is an efflux pump for various drugs. In this study, we assessed the involvement of other types of ABC transporters and exocytosis in the extracellular efflux of polymers from HeLa cells. The knockdown of various ABC transporters (ABCA1, ABCB1, ABCC1, and ABCG1) caused the intracellular amounts of all polymers at 24 h after micelle addition to increase when ABCB1 expression was suppressed, but not when ABCA1, ABCC1, or ABCG1 expression was

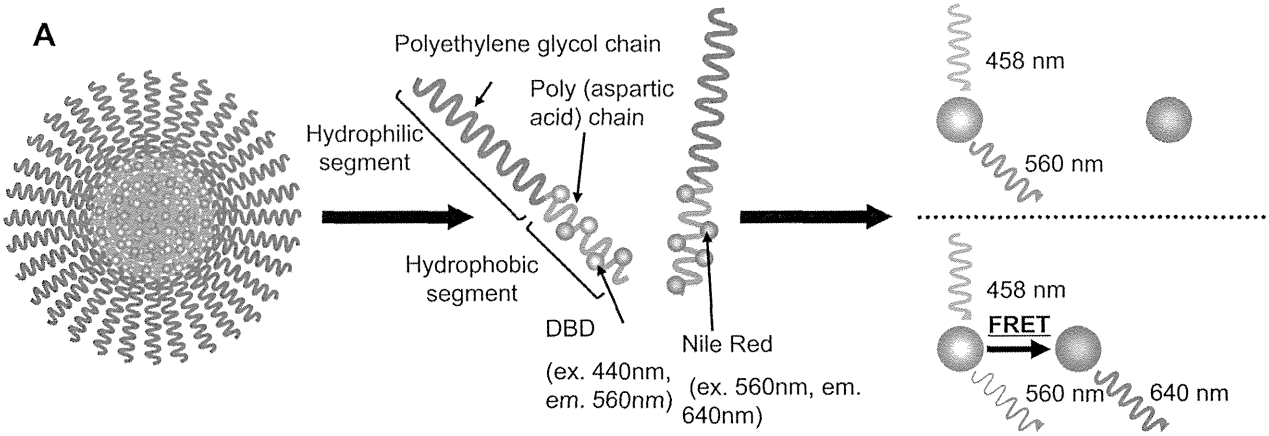

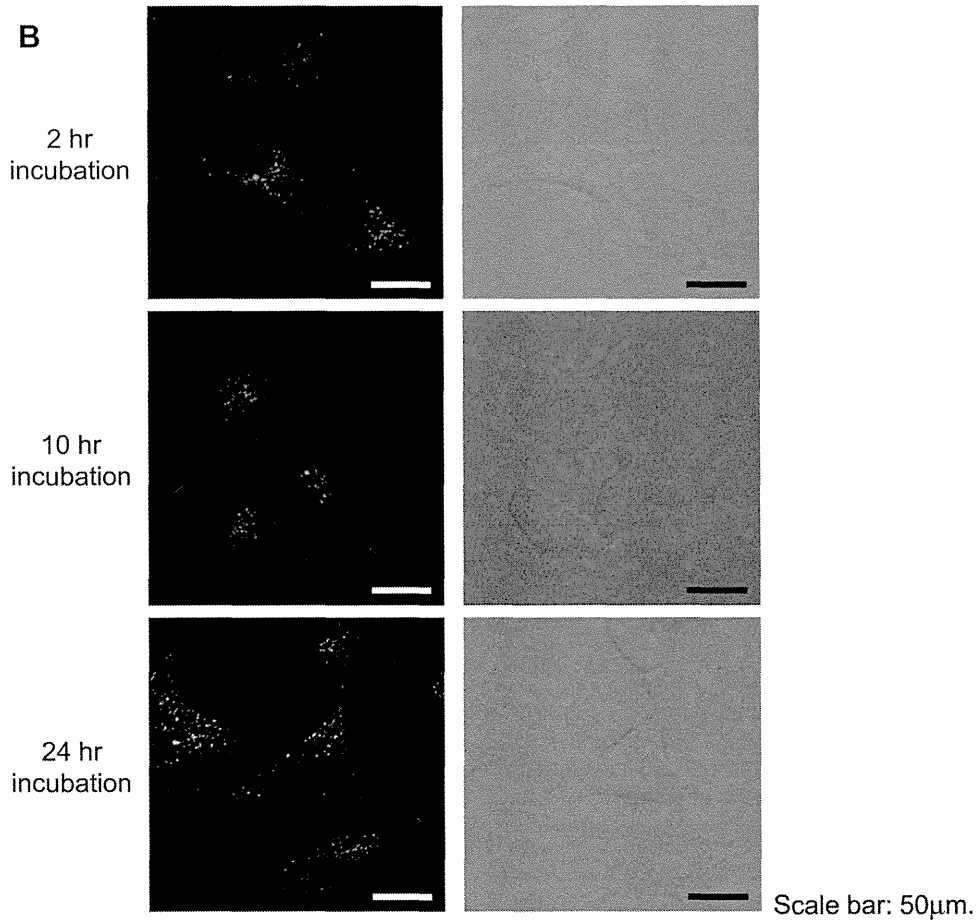

Fig. 3. (A) Schematic of FRET micelles used to investigate the structural integrity of micelles in HeLa cells. The fluorescent intensity of the donor, DBD (excitation 440 nm; emission 580 nm), enhanced the effective excitation of the acceptor, Nile Red (excitation 580 nm; emission 640 nm). (B) Confocal images of the fluorescent spectral shift that corresponds to the dissociation of FRET micelles. Cells were exposed to 50 μg/mL FRET micelles in culture medium. Two hours after the addition of micelles, the cells were washed and kept in medium without micelles; they were then subjected to confocal imaging at 2, 10, and 24 h after the addition of the micelles. Scale bars = 50 μm.

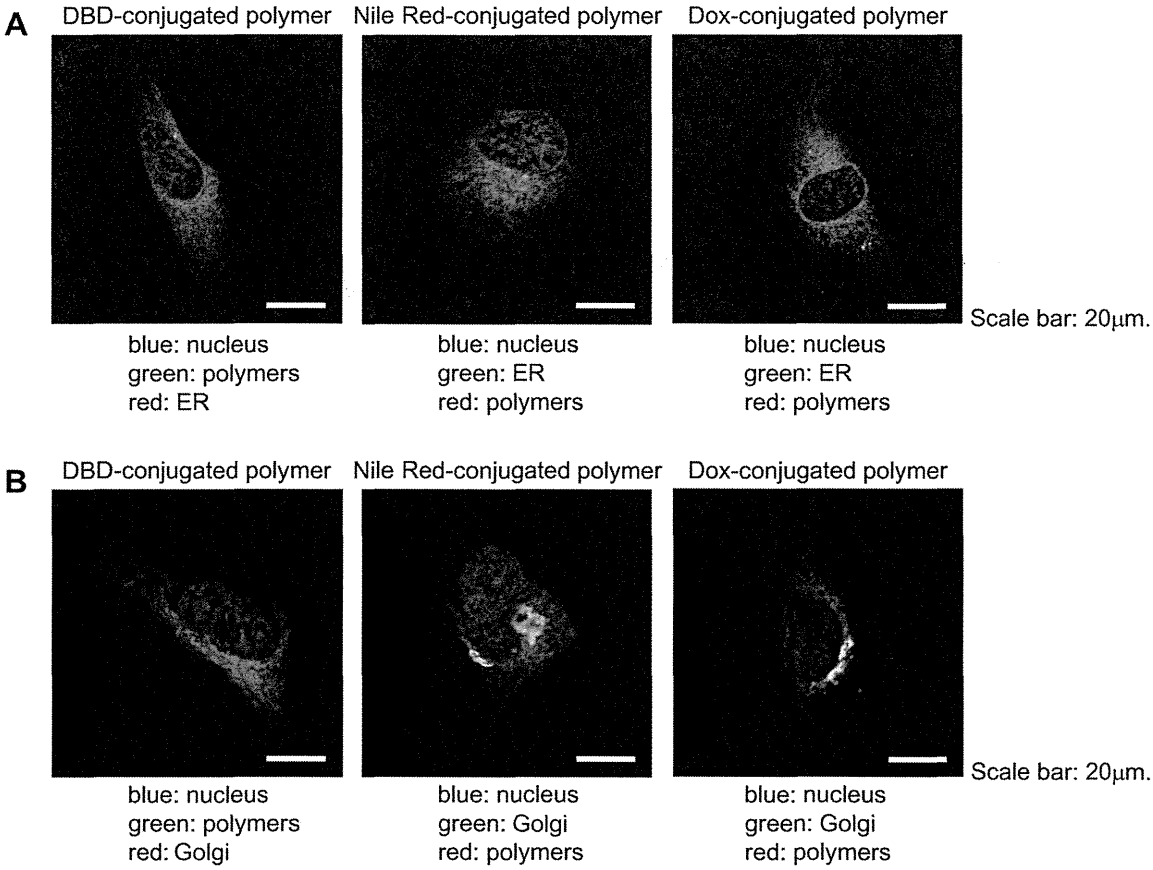

Fig. 4. Confocal images showing the intracellular localization of polymers at 24 h after the addition of micelles to HeLa cells. ER (A) and Golgi apparatus (B) were labeled with ER-Tracker and BODIPY-ceramide, respectively. Scale bars = 20 μm.

suppressed (Fig. 7A). On the other hand, the suppression of ABCB1 transporter expression did not lead to an increase in the intracellular amounts of dextran, polystyrene nanoparticle, or silica nanoparticle (Supplementary Fig. 5B).

With respect to exocytosis, the intracellular amounts of the polymers were also unaffected by the presence of snap-25, a known exocytosis-related protein (Fig. 7B).

3.7. *The transport of polymers by ABCB1*

The possibility remained that efflux only occurred for fluorescent compounds that were no longer conjugated to the polymers. Therefore, to further confirm the involvement of the ABCB1 transporter in the efflux of block copolymers, we used membranes expressing ABCB1. ATP-dependent transport increased at higher polymer concentrations for DBD-, Nile Red-, and Dox-conjugated polymers (Fig. 8A). All of the block polymers were transported through the membranes that expressed ABCB1, but were not transported through control membranes that lacked ABCB1 (Fig. 8B). To examine whether ABCB1 recognizes the conjugated fluorescent compounds or the polymer itself, we also examined the ATP-dependent transport of free DBD, Nile Red, and Dox and found that intravesicular uptake of DBD and Nile Red did not occur (Fig. 8C). Transport was observed for Dox, which is a well-known substrate of ABCB1. These findings indicate that the intravesicular fluorescence observed in our study and extracellular efflux observed in Fig. 7A did not stem from free fluorescent compounds, but rather from the fluorescent compounds conjugated to the polymers. Therefore, ABCB1 recognizes the block copolymer.

4. Discussion

The aim of this study was to elucidate the molecular mechanisms involved in the intracellular trafficking and extracellular efflux of block copolymer micelles and their components. In this study, we used block copolymer micelles conjugated with the fluorescent compounds Dox, DBD, and Nile Red.

The intracellular uptake of micelles was inhibited in the presence of chlorpromazine in HeLa cells (Fig. 2), suggesting that all micelles are taken up into the cells via clathrin-mediated endocytosis. However, caveolae-mediated endocytosis was also observed to some extent in all micelles as the incubation time progressed. The P85 amphiphilic triblock copolymer, which is composed of poly(ethylene oxide) (PEO) and poly(propylene oxide) (PPO), is internalized predominantly through caveolae-mediated endocytosis, although in the micelle form P85 is internalized exclusively through clathrin-mediated endocytosis [12,38].

FRET is a technique that has been used recently to measure the stability and dissociation of drug delivery system carriers and the release of encapsulated drugs. By using FRET micelles, we determined that micelle dissociation occurs within endosomes or lysosomes after internalization via endocytosis. This result indicates that the release of encapsulated drugs from these micelles will occur in endosomes or lysosomes.

We also investigated the molecular mechanisms involved in the intracellular trafficking of the block copolymers. When NPC1 expression was inhibited, the intracellular amounts of polymer increased (Fig. 5B). Confocal microscopy revealed that the knockdown of NPC1 expression suppressed the transport of the polymers

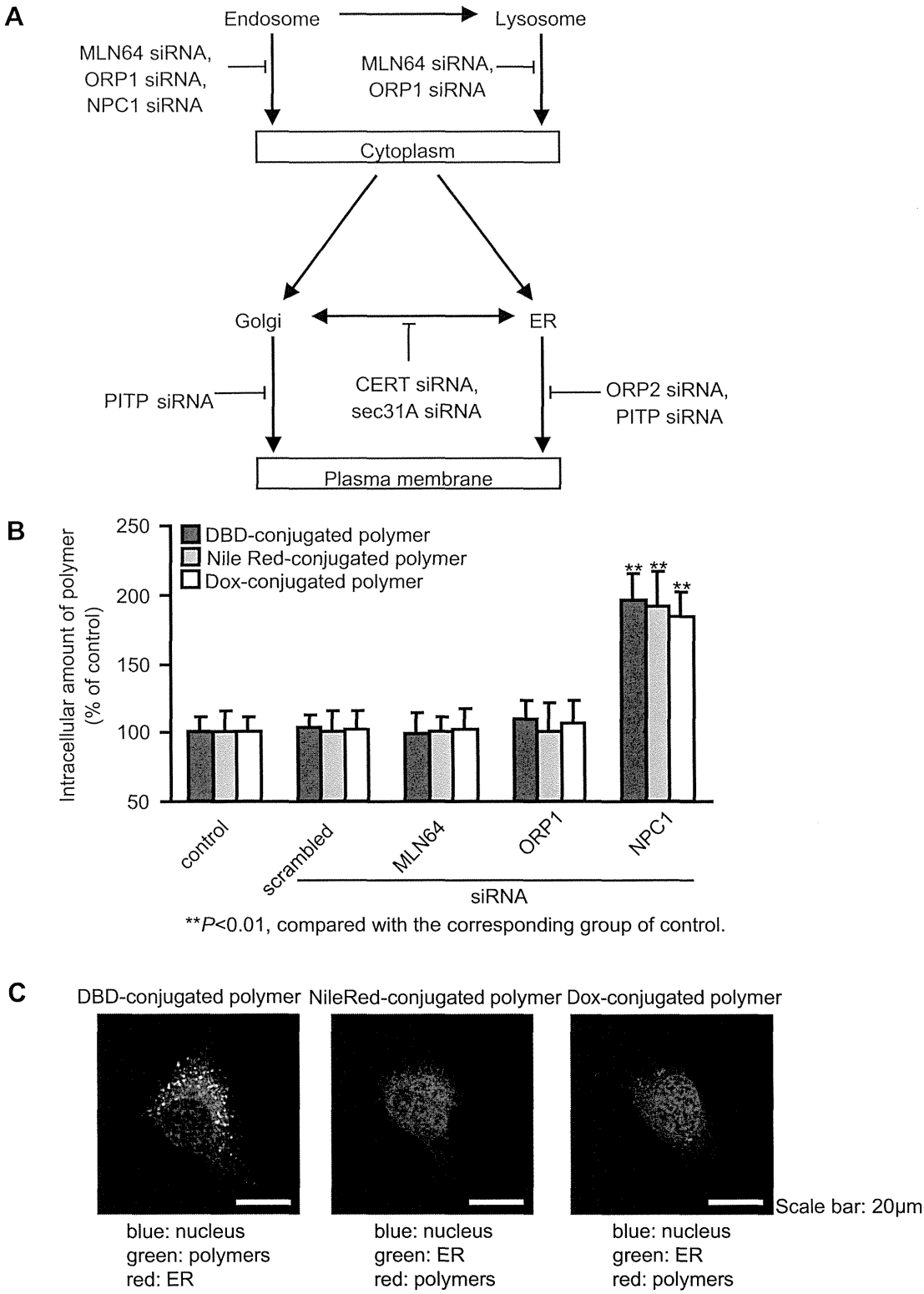

Fig. 5. (A) Intracellular components and typical lipid transport proteins. The expression of these proteins was suppressed by siRNA. (B) Intracellular amounts of polymers under suppressing conditions for each protein (MLN64, ORP1, and NPC1) at 24 h after the addition of micelles to HeLa cells. Cells were transfected with siRNAs against the targeted proteins by using Lipofectamine RNAiMAX according to the recommended protocols. $^{**}P < 0.01$ compared with the corresponding control group. Each value represents the mean ± SD ($n = 6$). (C) Confocal images showing the intracellular localization of micelles under suppressing conditions for NPC1 at 24 h after the addition of micelles to HeLa cells. The ER was labeled with ER-Tracker. Scale bars = 20 μm.